

# Global modelling of H<sub>2</sub> mixing ratios and isotopic compositions with the TM5 model

G. Pieterse<sup>1</sup>, M. C. Krol<sup>1,2</sup>, A. M. Batenburg<sup>1</sup>, L. P. Steele<sup>3</sup>, P. B. Krummel<sup>3</sup>, R. L. Langenfelds<sup>3</sup>, and T. Röckmann<sup>1</sup>

<sup>1</sup>Institute for Marine and Atmospheric Research Utrecht (IMAU), Utrecht, The Netherlands

<sup>2</sup>Department of Meteorology and Air Quality at Wageningen University, Wageningen, The Netherlands

<sup>3</sup>Centre for Australian Weather and Climate Research, CSIRO Marine and Atmospheric Research, Australia

Received: 1 December 2010 – Published in Atmos. Chem. Phys. Discuss.: 17 February 2011

Revised: 10 July 2011 – Accepted: 12 July 2011 – Published: 20 July 2011

**Abstract.** The isotopic composition of molecular hydrogen (H<sub>2</sub>) contains independent information for constraining the global H<sub>2</sub> budget. To explore this, we have implemented hydrogen sources and sinks, including their stable isotopic composition and isotope fractionation constants, into the global chemistry transport model TM5. For the first time, a global model now includes a simplified but explicit isotope reaction scheme for the photochemical production of H<sub>2</sub>. We present a comparison of modelled results for the H<sub>2</sub> mixing ratio and isotope composition with available measurements on seasonal to inter annual time scales for the years 2001–2007. The base model results agree well with observations for H<sub>2</sub> mixing ratios. For  $\delta D[H_2]$ , modelled values are slightly lower than measurements. A detailed sensitivity study is performed to identify the most important parameters for modelling the isotopic composition of H<sub>2</sub>. The results show that on the global scale, the discrepancy between model and measurements can be closed by adjusting the default values of the isotope effects in deposition, photochemistry and the stratosphere-troposphere exchange within the known range of uncertainty. However, the available isotope data do not provide sufficient information to uniquely constrain the global isotope budget. Therefore, additional studies focussing on the isotopic composition near the tropopause and on the isotope effects in the photochemistry and deposition are recommended.

## 1 Introduction

The role of molecular hydrogen (H<sub>2</sub>) as a possible energy carrier is an ongoing subject of debate in the political as well as the academic arena. In contrast to fossil fuels, which produce the long-lived greenhouse gas carbon dioxide (CO<sub>2</sub>) and other undesired compounds (e.g. carbon monoxide, nitrogen oxides and soot) upon oxidation with oxygen (O<sub>2</sub>), H<sub>2</sub> only produces water (H<sub>2</sub>O). Hence, using H<sub>2</sub> instead of fossil fuels could improve air quality and reduce the human impact on global climate. Unlike fossil fuels, H<sub>2</sub> is not available in large reservoirs, and the above mentioned positive effect can only be achieved if H<sub>2</sub> is produced from carbon-free resources.

In previous studies, potential adverse effects of the introduction of a hydrogen fuel economy were also identified. These effects are all related to the notion that a hydrogen fuel economy would lead to enhanced atmospheric mixing ratios of H<sub>2</sub> due to leakage in the production, distribution, storage and use of H<sub>2</sub>. H<sub>2</sub> is an important reaction partner of the hydroxyl radical (OH). Therefore, higher H<sub>2</sub> mixing ratios would consume OH radicals that would otherwise be available for the removal of other trace gases (Schultz et al., 2003), e.g. the greenhouse gas methane (CH<sub>4</sub>). Other studies investigated an adverse effect on the recovery of the ozone hole (Tromp et al., 2003; Warwick et al., 2004; Jacobson et al., 2005; Feck et al., 2008). Higher stratospheric H<sub>2</sub> mixing ratios lead to higher levels of stratospheric water vapour, which can result in increased formation of polar stratospheric clouds that would enhance polar ozone destruction.

The global H<sub>2</sub> cycle has been investigated by numerous studies, (e.g., Seiler and Conrad, 1987; Warneck, 1988; Ehhalt, 1999; Novelli et al., 1999; Hauglustaine and Ehhalt,



Correspondence to: T. Röckmann  
(t.roeckmann@uu.nl)

2002; Sanderson et al., 2003; Price et al., 2007; Yashiro et al., 2011) and the present state of knowledge has been recently reviewed by Ehhalt and Rohrer (2009), see Table 1 in Sect. 3.4.  $\text{H}_2$  is produced by the atmospheric oxidation of methane ( $\text{CH}_4$ ) and non methane hydrocarbons (NMHCs). Direct surface sources are from fossil fuel burning, biomass burning, and nitrogen fixation in the terrestrial biosphere and the oceans.  $\text{H}_2$  is removed by atmospheric oxidation and by dry deposition. Current estimates for the chemical lifetime of  $\text{H}_2$  vary between 1.4 and 2.3 yr, and for the total atmospheric burden between 141 and 172 Tg  $\text{H}_2$ . However, the uncertainties in the magnitudes of the different sources and sinks are even larger and call for further research.

Following the approach introduced by Gerst and Quay (2001), isotope measurements have been used to obtain further constraints on the individual source and sink strengths. The isotopic composition of methane-derived  $\text{H}_2$  was investigated by measurements in the stratosphere (Rahn et al., 2003; Röckmann et al., 2003; Rhee et al., 2006, 2008) as well as by detailed laboratory studies (Feilberg et al., 2004, 2005, 2007a,b; Rhee et al., 2008; Nilsson et al., 2007; Röckmann et al., 2010a; Nilsson et al., 2010). Isotope signatures for the surface sources are based on few early studies by Gerst and Quay (2001), and Rahn et al. (2002a,b, 2003). More detailed studies have been published very recently (Vollmer et al., 2010; Röckmann et al., 2010a). Price et al. (2007) were the first to implement the isotope signatures for  $\text{H}_2$  sources and sinks in a full global chemistry transport model. The actual isotope chemistry involved with the oxidation of  $\text{CH}_4$  and the NMHCs was not implemented but the resulting isotopic  $\delta\text{D}[\text{H}_2]$  signature of the photochemical source of  $\text{H}_2$  was optimised to a value of  $+162^{+57}_{-57}$ ‰ to close the isotope budget. In this work, the values for  $\delta\text{D}[\text{H}_2]$  are calculated from the ratio  $R = \text{D}/\text{H}$  as  $\delta\text{D}[\text{H}_2] = (R/R_{\text{VSMOW}} - 1)$ , where  $R_{\text{VSMOW}} = 1.558 \times 10^{-4}$  is the reference D/H ratio of Vienna Standard Mean Ocean Water. How the various isotopologues progress through the  $\text{CH}_4$  and NMHC oxidation chain, however, is still an open question.

In a recent study, Pieterse et al. (2009) derived and evaluated a hydrogen isotope chemistry scheme including the full methane oxidation chain and a condensed NMHC oxidation scheme. The findings of the experimental studies by Feilberg et al. (2004, 2005, 2007a,b); Nilsson et al. (2007, 2010) and Rhee et al. (2008) were incorporated into the resulting model framework. The result was a chemistry scheme that is internally consistent with respect to the derived kinetic isotope effects (KIEs), and the isotopic branching (IB) ratios. This work describes the implementation of this new isotope chemistry scheme in version 5 of the global Transport Model (TM5) developed by Krol et al. (2005), summarised in Sect. 2. In contrast to previous studies, this implementation allows for a detailed analysis of the full  $\text{H}_2$  cycle, including its stable isotopologue HD because the isotopic composition of the intermediate compounds and the enrichment due to the oxidation of  $\text{CH}_4$  and the NMHCs are explicitly calculated.

Furthermore, the sensitivity of the isotopic composition to changes in the initial isotopic composition of  $\text{CH}_4$  and the NMHCs, or to changes in the isotope kinetics in each relevant reaction step of the photochemical pathway from  $\text{CH}_4$  to  $\text{H}_2$  can be calculated. With the implementation of the explicit isotope scheme in TM5, the global budgets of  $\text{H}_2$  and HD can be fully assessed.

In Sect. 3, the modelled  $\text{H}_2$  mixing ratios are compared with available measurements from the National Oceanic and Atmospheric Administration (NOAA), reported in Novelli et al. (1999), the Australian Commonwealth Scientific and Research Organisation (CSIRO), and the Advanced Global Atmospheric Gases Experiment (AGAGE), both reported in Xiao et al. (2007). Measurements provided by Rice et al. (2010) and by the Eurohydros project (Batenburg et al., 2011) are used to evaluate the modelled isotopic composition of  $\text{H}_2$ . After the comparison with available experimental data, the spatial vertical and surface patterns of the  $\text{H}_2$  mixing ratio and isotopic composition are analysed. Finally, the global  $\text{H}_2$  isotope budget and its sensitivity to changes in the parameters of the main processes, e.g. deposition, photochemistry, and the stratosphere-troposphere exchange (STE) are investigated. The overall conclusions are summarised in Sect. 4.

## 2 Model adaptations

### 2.1 Implementing condensed methane isotope chemistry

The chemistry in the TM5 model (Krol et al., 2005) is described by the Carbon Bond Mechanism 4 (CBM-4) introduced by Houweling et al. (1998). We have added the hydrogen isotope scheme described by Pieterse et al. (2009), thus extending the original CBM-4 reaction scheme by the important intermediate singly deuterated isotopologues ( $\text{CH}_2\text{DOO}$ ,  $\text{CH}_2\text{DOOH}$ ,  $\text{CHDO}$ , and  $\text{HD}$ ). This allows investigating for the first time the contributions of the individual reaction steps in the methane and NMHC oxidation chains to the final overall isotopic signature of the photochemical source of  $\text{H}_2$  in the troposphere. The detailed derivation and implementation of the  $\text{CH}_4$  reaction scheme is provided in Appendix A.

### 2.2 Implementing NMHC isotope chemistry

The non methane hydrocarbon (NMHC) chemistry was also adopted from CBM-4, and the photochemical NMHC chemistry scheme was extended with the singly deuterated hydrogen isotope chemistry described by Pieterse et al. (2009), further described in Appendix B. A serious shortcoming for  $\text{H}_2$  isotope modelling is that almost no information is available about the isotopic composition of the atmospheric NMHCs. The NMHC measurements themselves are difficult and in many cases just being developed and therefore almost no systematic atmospheric investigations exist. For the present

**Table 1.** Global budget of H<sub>2</sub> from the TM5 reference model run (numbers in Tg H<sub>2</sub> per year).

	Novelli et al. (1999)	Hauglustaine and Ehhalt (2002)	Sanderson et al. (2003)	Rhee et al. (2006)	Price et al. (2007)	Xiao et al. (2007)	Ehhalt and Rohrer (2009)	Yashiro et al. (2011)	This work
<b>Sources</b>									
Fossil fuel	15	16	20.0	15	18.3	15	11	15.1–15.4	17.0 <sup>+3</sup> <sub>-6</sub>
Biomass burning	16	13	20.0	16	10.1	13	15	8–15	15.0 <sup>+3</sup> <sub>-3</sub>
Biofuel					4.4				
Ocean N <sub>2</sub> fixation	3	5	4.0	6	6.0		6	6	5.0 <sup>+1</sup> <sub>-2</sub>
Land N <sub>2</sub> fixation	3	5	4.0	6	0.0		3	3	3.0 <sup>+3</sup> <sub>-3</sub>
Photochemical production	40	31	30.2	64	34.3	77	41	36–37	37.3
<b>Total</b>	<b>77</b>	<b>70</b>	<b>78.2</b>	<b>107</b>	<b>73.1</b>	<b>105</b>	<b>76</b>	<b>69–76</b>	<b>77.3</b>
<b>Sinks</b>									
Photochemical removal	19	15	17.1	19	18.0	18	19	17–18	22.1
Deposition	56	55	58.3	88	55.0	85	60	54–57	55.8
<b>Total</b>	<b>75</b>	<b>70</b>	<b>75.4</b>	<b>107</b>	<b>73.0</b>	<b>105<sup>a</sup></b>	<b>79</b>	<b>73–76</b>	<b>77.9</b>
Tropospheric burden (Tg H <sub>2</sub> )	155	136	172 <sup>b</sup>	150 <sup>c</sup>	141	149	155 <sup>d</sup>	150	169 <sup>e</sup>
Tropospheric lifetime (yr)	2.1	1.9	2.2 <sup>b</sup>	1.4	1.9	1.4	2.0	2	2.2 <sup>e</sup>

<sup>a</sup> Includes export to stratosphere of 1.9 Tg H<sub>2</sub> per year.

<sup>b</sup> The model domain for the budget calculation reached 100 hPa. For the troposphere with a mass of 0.82 of the total atmosphere the burden would be 157 Tg H<sub>2</sub> and the tropospheric lifetime 2.0 yr.

<sup>c</sup> Calculated from sources and lifetime.

<sup>d</sup> From Novelli et al. (1999).

<sup>e</sup> The model domain for the budget calculation runs from the surface to 100 hPa. For the troposphere with a mass of 0.82 of the total atmosphere the burden would be 155 Tg H<sub>2</sub> and the lifetime 2.0 yr.

study, we have chosen to deliberately set the D/H isotope ratio of NMHCs to the average value for methane (−86 ‰), although in reality, the isotopic composition of these species might be lower. It would be useful to link the information available on bio synthesis of natural compounds from the field of biochemistry (e.g., Schmidt et al., 2003) to the atmosphere, but this is beyond the scope of this work. Because the atmospheric lifetime of most hydrocarbons is short, the singly deuterated companion species are not explicitly defined and transported in TM5. The reaction mass fluxes of the deuterated product species, such as deuterated formaldehyde, are calculated by correcting the mass fluxes of the non-deuterated product species using the above mentioned assumption for the initial isotopic composition. This means that for this initial study we also neglect the potential spatial and temporal variability of the isotopic composition of the NMHC species.

### 2.3 Parameterisation of the stratospheric H<sub>2</sub> composition

The TM5 model is primarily designed for modeling tropospheric chemistry, although a version focusing on stratospheric chemistry exists (van den Broek et al., 2003). Hence, the implementation of the stratospheric chemistry is rather crude and does not consider, for example, the oxidation of methane by chlorine radicals (Cl), and electronically excited oxygen atoms, O(<sup>1</sup>D). Therefore, it is not possible to implement a stratospheric reaction scheme for H<sub>2</sub> – like presented

by Rahn et al. (2003) and Röckmann et al. (2003). Instead, we implemented an empirical linear parametrisation of HD relative to CH<sub>4</sub> as proposed by McCarthy et al. (2004) for the stratosphere. The following latitude ( $\theta$ ) dependent threshold pressure level  $p_s$  (Pa) separates the troposphere and the stratosphere:

$$p_s = 3.00 \times 10^4 - 2.15 \times 10^4 \cos(\theta). \quad (1)$$

For all pressures below the threshold pressure level, the CBM-4 mixing ratios for H<sub>2</sub> and HD chemistry are replaced by the empirical parametrisation. Because H<sub>2</sub> and HD are transported as separate species, the TM5 model requires an explicit expression for the mixing ratio of both species as a function of CH<sub>4</sub>, which is derived from the results of McCarthy et al. (2004). The four-dimensional variational (4-D-Var) data assimilation system implemented in TM5 (Meirink et al., 2008a,b) was used to obtain the background CH<sub>4</sub> mixing ratios for the troposphere as well as the stratosphere. In order to constrain the H<sub>2</sub> mixing ratio and isotopic composition at the tropopause to 530 ppb and +130 ‰, the original HD-CH<sub>4</sub> relation was slightly modified (units in ppb):

$$[\text{HD}] = -6.32 \times 10^{-5} [\text{CH}_4] + 0.301. \quad (2)$$

For  $\delta\text{D}[\text{H}_2]\text{-CH}_4$ , the data presented in Rahn et al. (2003); McCarthy et al. (2004) yield (units in ‰):

$$\delta\text{D}[\text{H}_2] = -0.267 [\text{CH}_4] + 610. \quad (3)$$

These expressions fit the experimental data within the typical range of uncertainty of  $\pm 1\%$  for the H<sub>2</sub> mixing ratios, and

$\pm 10\%$  for the isotopic compositions. The stratospheric  $\text{H}_2$  mixing ratio is then approximated by:

$$[\text{H}_2] = \frac{1}{2(\delta\text{D}[\text{H}_2] + 1)R_{\text{VSMOW}}}[\text{HD}]. \quad (4)$$

The factor 2 accounts for the fact that the isotopic composition is measured at a per atom basis, while there are two hydrogen atoms in the hydrogen molecule. Doubly deuterium substituted molecules are neglected in this study.

## 2.4 Implementing the surface sources

In the original implementation, TM5 uses the EDGAR3.2 inventory (Olivier and Berdowski, 2001) for the surface sources. The spatial distributions and relative magnitudes of the hydrogen surface emissions required for the calculations were obtained from Schultz and Stein (2006). However, exploratory calculations with the original source magnitudes produced results that systematically underestimated the measured hydrogen mixing ratios. Therefore, we decided to scale the different source fluxes to the average of previously reported global budget estimates (Novelli et al., 1999; Hauglustaine and Ehhalt, 2002; Sanderson et al., 2003; Rhee et al., 2006; Price et al., 2007; Xiao et al., 2007; Ehhalt and Rohrer, 2009; Yashiro et al., 2011), resulting in the values shown in Tables 1 and 2 in Sect. 3.4. The upper and lower bounds of the averaged surface source magnitude estimates are also shown in the tables. The reported uncertainties in the individual papers are generally larger; up to  $\pm 10 \text{ Tg yr}^{-1}$  for the fossil fuel emissions and biomass burning, and up to  $\pm 5 \text{ Tg yr}^{-1}$  for  $\text{H}_2$  released from ocean and land  $\text{N}_2$  fixation. The isotopic signatures were adopted from Price et al. (2007).

## 2.5 Deposition parametrisation

The deposition scheme implemented in TM5, originally adopted from Ganzeveld et al. (1998) was extended for  $\text{H}_2$  and HD by implementing the surface resistance parametrisation for deposition of  $\text{H}_2$  reported by Conrad and Seiler (1980, 1985); Yonemura et al. (2000); Sanderson et al. (2003). It distinguishes between seven ecosystem types: Savannah, Agricultural, Forest, Grasslands/Prairies, Peat/Tundra, Semi-desert, and Desert. The first four include soil moisture dependency. The different ecosystem types were assigned to the land use types defined by the European Centre for Medium-Range Weather Forecasts (ECMWF) that are implemented in the TM5 model. Typical deposition velocities vary between 0 and  $1.3 \text{ mm s}^{-1}$  in accordance with the above mentioned studies. In preliminary calculations with this scheme, the modelled  $\text{H}_2$  NH mixing ratios were underestimated by about 10%. Decreasing the overall deposition velocity by the same amount resulted in the optimal agreement between the model and available data. This adaptation is justifiable because the corrected values are still well

within the reported ranges of uncertainty (more than  $\pm 15\%$  for the underlying deposition measurements).

The deposition scheme implemented in TM5 is an inferential deposition model (e.g., Garland, 1977; Hicks et al., 1991). The deposition flux  $F_C$  of a certain chemical species  $C$  to the surface is calculated as the difference between the ambient and surface mixing ratio ( $[C]_{\text{a}}$  and  $[C]_0$ , respectively) multiplied with the deposition velocity of the chemical species,  $v_d$ :

$$F_C = -v_d([C]_{\text{a}} - [C]_0). \quad (5)$$

Generally,  $[C]_0$  is assumed zero so that only removal takes place. The overall resistance to deposition ( $R_t \equiv 1/v_d$ ) is the series resistance sum of the aerodynamic resistance ( $R_a$ ), which accounts for the turbulent diffusion in the surface layer, the quasi-laminar boundary-layer resistance ( $R_b$ ), which accounts for the molecular diffusion through the layer just above the surface layer, and finally the surface resistance ( $R_s$ ). Typically,  $R_s$  is the parallel resistance sum of the vegetation deposition resistance ( $R_{\text{veg}}$ ) and the soil deposition resistance ( $R_{\text{soil}}$ ), see for example Ganzeveld and Lelieveld (1995); Ganzeveld et al. (1998); Meyers et al. (1998). Technically, the chamber measurements performed by Gerst and Quay (2001) to determine the fractionation of the deposition process were conducted for conditions in which  $R_a \ll R_b + R_s$ . Moreover, turbulent diffusion, represented by  $R_a$ , will not introduce fractionation. However, in the majority of the field studies the total resistance is reported and therefore, we chose to implement an overall fractionation constant for the reference scenario calculations, i.e. the deposition velocity of HD was calculated by multiplying the resulting  $\text{H}_2$  deposition velocity with the overall fractionation constant of 0.943 for hydrogen deposition (Gerst and Quay, 2001).

## 3 Analysis of model results

### 3.1 Comparison with $\text{H}_2$ mixing ratio measurements

Calculations were performed with a resolution of 6 by 4° (longitude-latitude) for the years 2001 to 2007 to ensure sufficient overlap with available measurements. Prior to producing the results presented here spin up calculations were performed until both the mixing ratios as well as the isotopic compositions were sufficiently converged. Due to changes in the ECMWF native model, that is used to drive the atmospheric transport, the results for the years 2001–2005 were calculated using 25 vertical levels, whereas the results for 2006 and 2007 were obtained using 34 vertical levels. In this section, we compare the modelled  $\text{H}_2$  mixing ratio fields with available measurements.

Figure 1 shows the comparison of the model results for Alert (Canada) and the South Pole. For Alert, the seasonal signals are captured reasonably well. The large variability (generally  $\text{H}_2$  depletion) in the measured mixing ratio at

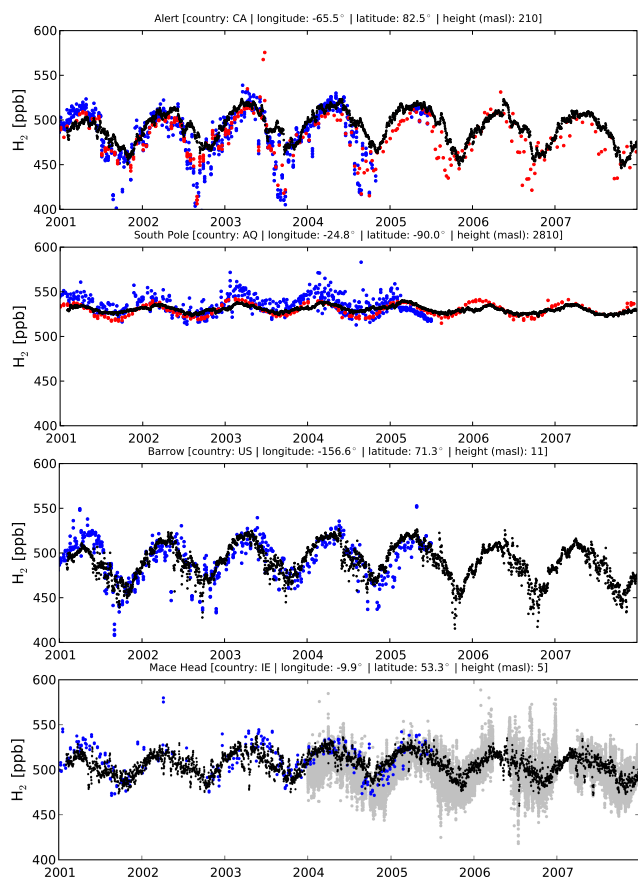


**Fig. 1.** Comparison between the measured background and modelled (black) noon-time  $H_2$  mixing ratios at Alert, the South Pole, Barrow and Mace Head. Available measurements from NOAA, CSIRO and AGAGE are shown in blue, red, and grey, respectively. Measurements from AGAGE are shown without filtering for background conditions.

Alert is caused by soil uptake of  $H_2$  from the air masses arriving from the westerly direction due to deposition in the northern part of Russia during the northern hemispheric summer and autumn season. These events are not reproduced by the model, which shows that deposition is likely underestimated. Such variability is absent at the South Pole because there is no ice-free land surface around the station. Note that the model assumes that there is no deposition to snow and ice. The figure shows good agreement for the stations at Barrow (Alaska) and Mace Head (Ireland). At the resolution used for the calculations, the model cannot capture the variability in the mixing ratios caused by local influences, but the seasonal cycles are adequately reproduced.

The measurements from Ascension Island (Atlantic Ocean) are characterised by little variability, as shown in Fig. 2. This station is hardly influenced by deposition and surface sources because it is situated far away from the major land masses. For Cape Grim (Tasmania), the model results show much more variability than the baseline values reported by NOAA and CSIRO. However, the comparison with the

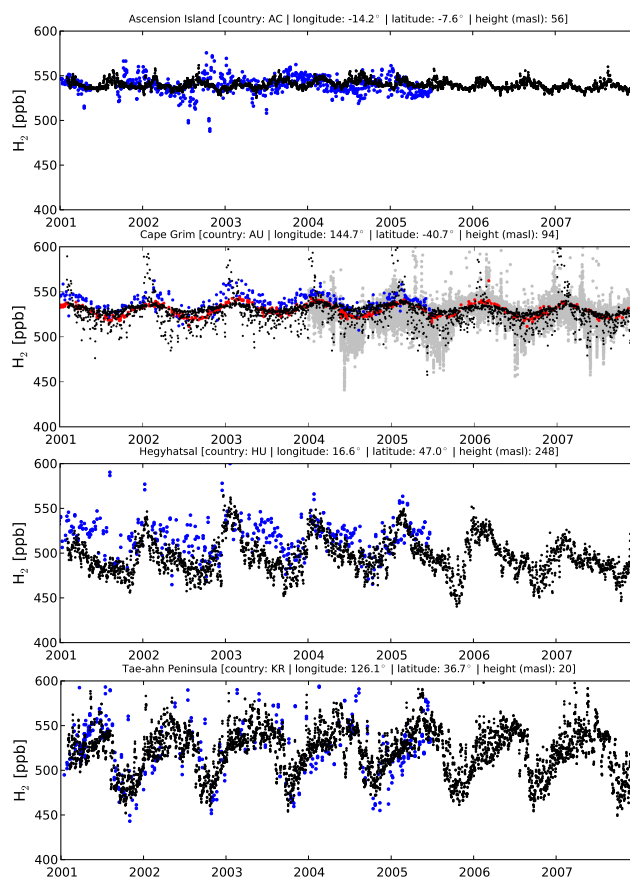


**Fig. 2.** Comparison between the measured and modelled (black) noon-time  $H_2$  mixing ratios at Ascension Island, Cape Grim, Hegyhatsal and the Tae-Ahn peninsula. Available measurements from NOAA, CSIRO and AGAGE are shown in blue, red, and grey, respectively. Measurements from AGAGE are shown without filtering for background conditions.

continuous AGAGE measurements shows that the unfiltered variability is even larger than predicted by the model. The stations at Hegyhatsal (Hungary) and the Tae-Ahn peninsula (Republic of Korea) are highly influenced by local processes. The former is a continental station primarily influenced by biogenic processes whereas the latter is located in the highly polluted area in East Asia. Nevertheless, the model is able to capture the measured variability rather well for both stations.

Summarising, the model performs well in predicting the measured mixing ratios at background and continental stations, both in the NH as well as in the SH. This suggests that the modelled  $H_2$  budget and the magnitudes of the different sources and sinks are reasonable. This provides an excellent starting-point for the evaluation of the isotopic composition in the next section, where we will compare the modelled results with available data. The agreement between the model results and the measurements was also observed for 39 other sites from the NOAA and CSIRO networks. The remaining comparisons are available in the Supplement.

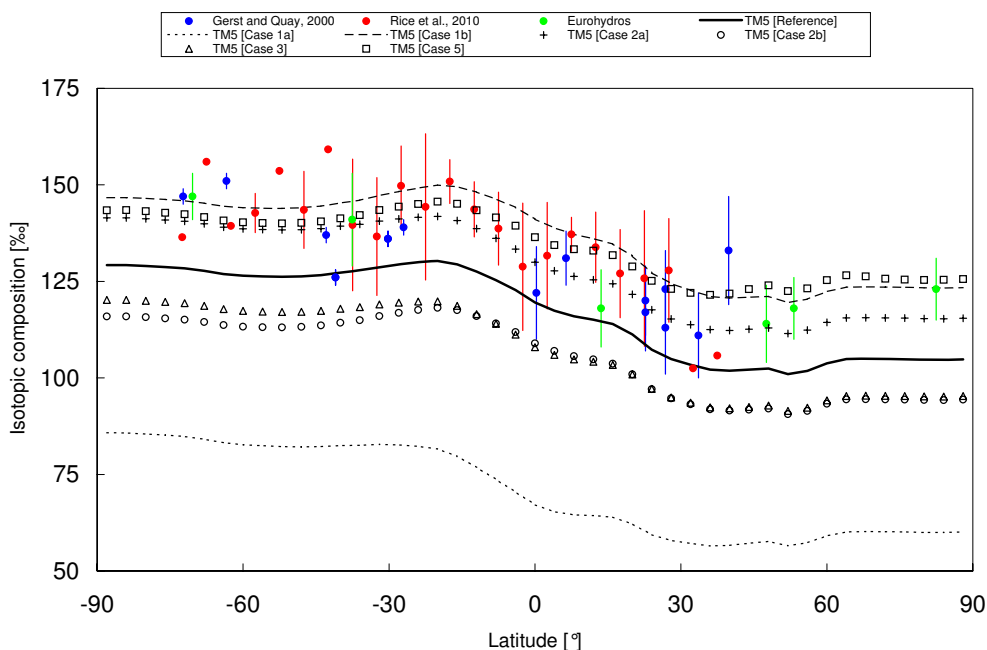


**Fig. 3.** Comparison of the modelled zonal mean surface isotopic composition (thick solid line) with available measurements. Blue circles represent measurements from Gerst and Quay (2000), red circles represent measurements from Rice et al. (2010), and green circles represent measurements from the Eurohydros project (Batenburg et al., 2011). Also shown are some of the cases of the sensitivity study discussed in Sect. 3.6. Case 1a shows the effect of using the KIEs for formaldehyde photolysis as proposed by Feilberg et al. (2007a), case 1b shows the effect of changing the pressure dependency of the molecular photolysis channel for formaldehyde, case 2a shows the effect of increasing the stratospheric isotopic composition by 20 ‰, case 2b shows the effect of shifting the tropopause pressure level, case 3 shows the effect of decreasing the isotopic composition of the primary NMHCs to  $-200$  ‰, and case 5 shows the effect of reducing the deposition fractionation constant to 0.900.

### 3.2 Comparison with $H_2$ isotope measurements

In Fig. 3, the latitudinal gradient of zonal mean values from the TM5 model is compared to measurements from Gerst and Quay (2000), Rice et al. (2010) and samples from the Eurohydros project for which the  $H_2$  mixing ratios can also be found in Batenburg et al. (2011). The results for the reference scenario (thick solid line) show a systematic negative bias in the isotopic composition of about 10–20 ‰. This deviation is relatively small compared to the uncertainties in the fluxes and isotopic composition of the sources and sinks that contribute to the final isotopic composition (see Table 2). Furthermore, it should be noted that the measurements usually represent air of non-continental origin, whereas the model averages over a latitude band and therefore includes in the average also  $H_2$  emitted from the isotopically depleted sources over land. Thus, the available isotope measurements are not necessarily representative for the whole latitude band and the background isotope measurements are expected to be slightly more enriched. Additional measurements at non-background locations (e.g. regions dominated by deposition or surface sources) would be useful to investigate the spatial distribution in more detail. With the data presently available, the comparison shows that the global isotope budget is already

reasonably well described by the reference scenario. The sensitivity of the results to a number of model parameters is discussed in more detail in Sect. 3.6.

Figure 4 shows time series of the modelled (monthly averaged) and measured isotopic composition at the 6 Eurohydros flask stations (Batenburg et al., 2011) for the years 2006 and 2007. The corresponding measured  $H_2$  mixing ratios can be found in Batenburg et al. (2011). In general, the modelled isotope results are slightly depleted compared to the measurements, as discussed above. However the differences are not uniform between the stations. The largest underestimate is found at Neumayer. Here, the model also predicts a small but clear seasonal cycle with an amplitude of  $\sim 10$  ‰, which is not discernible in the data. At Amsterdam Island, the discrepancy between model and data is somewhat reduced. Similar to Neumayer, the scatter in the data is too high to detect/verify a possible seasonal cycle. Cape Verde Island is the station where the model captures the measured values best. Unfortunately, the record for direct comparison is shortest, but the absolute values and the seasonal differences seem to be well represented by the model. The measurements at the continental station Schauinsland show the highest degree of variability due to influences from surface sources and deposition. The model averages out much of this variability

**Table 2.** Global isotope budget of H<sub>2</sub> up to 100 mbar.

	Magnitude (Tg H <sub>2</sub> yr <sup>-1</sup> )	Signature a	Relative signature b	Composition (‰)
<b>Sources</b>				
Fossil fuel <sup>c</sup>	17.0 <sup>+3</sup> <sub>-6</sub>	-196 <sup>+10</sup> <sub>-74</sub>	2.754 × 10 <sup>-5</sup>	
Biomass burning <sup>d</sup>	15.0 <sup>+5</sup> <sub>-5</sub>	-260 <sup>+60</sup> <sub>-60</sub>	2.237 × 10 <sup>-5</sup>	
Ocean N <sub>2</sub> fixation <sup>e</sup>	5.0 <sup>+1</sup> <sub>-2</sub>	-628 <sup>+0</sup> <sub>-72</sub>	3.748 × 10 <sup>-6</sup>	
Land N <sub>2</sub> fixation <sup>e</sup>	3.0 <sup>+3</sup> <sub>-3</sub>	-628 <sup>+0</sup> <sub>-72</sub>	2.249 × 10 <sup>-6</sup>	
Photochemical production <sup>f</sup>	37.3	+116	8.391 × 10 <sup>-5</sup>	
Total	77.3		1.398 × 10 <sup>-4</sup>	
<b>Sinks</b>				
Photochemical removal <sup>g</sup>	22.1	0.542	0.154	
Deposition <sup>g</sup>	55.8	0.925	0.663	
Total	77.9		0.817	
<b>Isotopic composition</b>				
From budget				99
Modelled composition				128
Stratospheric contribution				29

<sup>a</sup> Sources are expressed in ‰, sinks are expressed in fractionation constants.

<sup>b</sup> Source or sink signature weighted by the flux magnitude. Here, sources are expressed as flux weighted isotope ratios (*R*).

<sup>c</sup> Source signature from Gerst and Quay (2001). Combined range of uncertainty includes the value of -270 ‰ reported by Rahn et al. (2002b).

<sup>d</sup> Source signature from Gerst and Quay (2001).

<sup>e</sup> Source signature from Price et al. (2007). Combined range of uncertainty includes the value of -700 ‰ reported by Rahn et al. (2003).

<sup>f</sup> Calculated from model results.

<sup>g</sup> Calculated from model results by Eq. (7).

and predicts a rather small seasonal cycle disturbed by local variability. At Mace Head, the model captures the phase and amplitude of the seasonal cycle in 2007 very well, but again with a negative bias. Some measurements in summer 2006 appear anomalously high compared to the model and the 2007 record, but in general the agreement is very good. This deteriorates again when going to the high northern latitudes. Whereas the model predicts a rather similar seasonality as in Mace Head, the measurements show a shift in the phase for Alert. Direct comparison of the data for Alert and Mace Head in Fig. 4 shows that at Alert,  $\delta D[H_2]$  values increase again after the seasonal minimum 1–2 months earlier than at Mace Head. Possibly, the phase shift in the modelled and measured seasonal signals at Alert is caused by the implementation of the deposition scheme for snow-covered conditions. In the current model deposition parametrisation, no deposition will occur in (partly) snow covered regions. It is therefore possible that in reality, deposition will start affecting the isotopic composition much earlier in the season than expected from the model results. Indeed, the mixing ratios for Alert in Fig. 1 already showed that the modelled seasonal minimum in the H<sub>2</sub> mixing ratio is delayed compared to seasonal minimum in the observations by a similar period. Moreover, the modelled H<sub>2</sub> seasonal minimum in the mixing ratio is significantly higher than the observed

minimum mixing ratio, which leads to an underestimate in the modelled isotopic composition. Hence, more deposition measurements in continental regions like Siberia (the area of influence for Alert) could help to improve our insight into the northern hemispheric H<sub>2</sub> cycle.

This qualitative comparison shows that there are potentially interesting isotope signals in the detailed records at individual measurement stations close to H<sub>2</sub> sources and sinks, but for the analysis in this paper we focus on the global values (e.g. Fig. 3). The difference between the model results and measurements appears limited for the tropics (i.e. ~0–5 ‰ at Cape Verde), increases with latitude, and is more pronounced at the Southern Hemisphere (~20 ‰) than on the Northern Hemisphere (~10–20 ‰). Because the photochemical production of H<sub>2</sub> is a strong source in the tropics, the agreement in the tropics suggests that the modelled tropospheric photochemical source signature is roughly realistic. However, one has to keep in mind that the global comparison also depends on the representativeness of the zonal average when compared to point measurements in the tropics. As the figures in the next section will show, there is a large variability caused by the sources and sinks in the tropics around the globe.

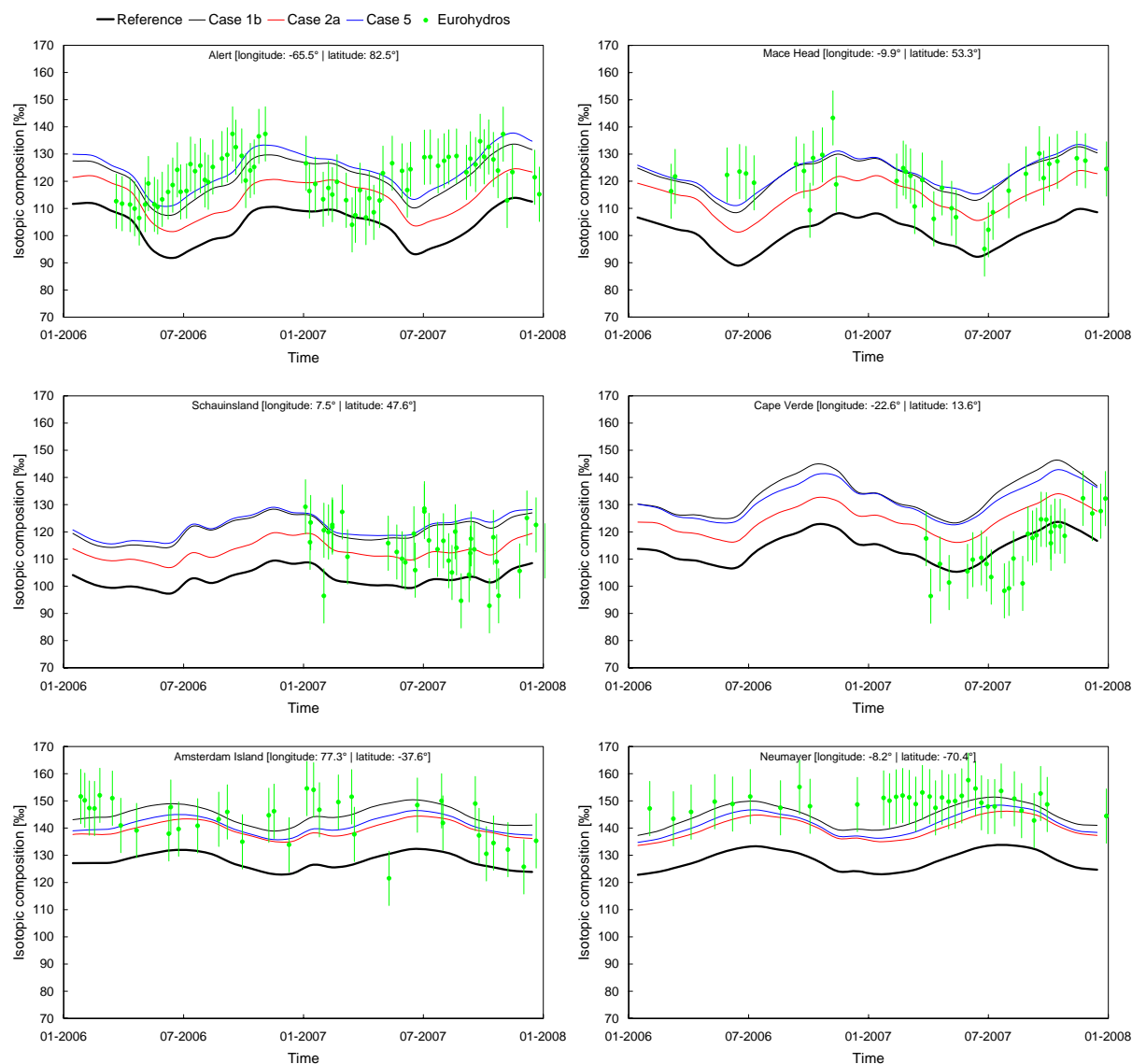


**Fig. 4.** Comparison of the modelled isotopic composition (thick black) with available measurements (green) from Alert, Mace Head, Schauinsland, Cape Verde, Amsterdam Island, and Neumayer. The corresponding  $\text{H}_2$  mixing ratios can be found in Batenburg et al. (2011). Also shown are some of the cases of the sensitivity study discussed in Sect. 3.6. case 1b (thin black) shows the effect of changing the pressure dependency of the molecular channel of formaldehyde removal by photolysis, case 2a (red) the effect of increasing the stratospheric isotopic composition by 20 ‰, and case 5 (blue) the effect of changing the deposition fractionation constant to 0.900.

### 3.3 Spatial patterns of $\text{H}_2$ mixing ratios and isotopic compositions

The left column in Fig. 5 shows the modelled latitude-altitude fields of  $\text{H}_2$  mixing ratio for different seasons. Latitudinal, vertical and temporal variability is generally small in the southern extratropics. The  $\text{H}_2$  mixing ratio in the tropics reaches a maximum during the northern hemispheric spring and summer, which penetrates deep into the free troposphere. In the northern extratropics,  $\text{H}_2$  mixing ratios are lowest year-round and show a strong seasonal minimum in the fall season

(SON). The vertical gradient is small in the Southern Hemisphere but quite substantial in the Northern Hemisphere, confirming earlier findings of Hauglustaine and Ehhalt (2002) and Price et al. (2007).

The corresponding isotopic compositions are shown in the right column of Fig. 5. The dominant effect in this view is the strong enrichment of  $\text{H}_2$  in the stratosphere. This overshadows the smaller temporal and latitudinal changes in the troposphere. In general, the NH is depleted in D compared to the SH, as shown above. In the northern extratropics and tropics, there is generally only a weak vertical gradient in the

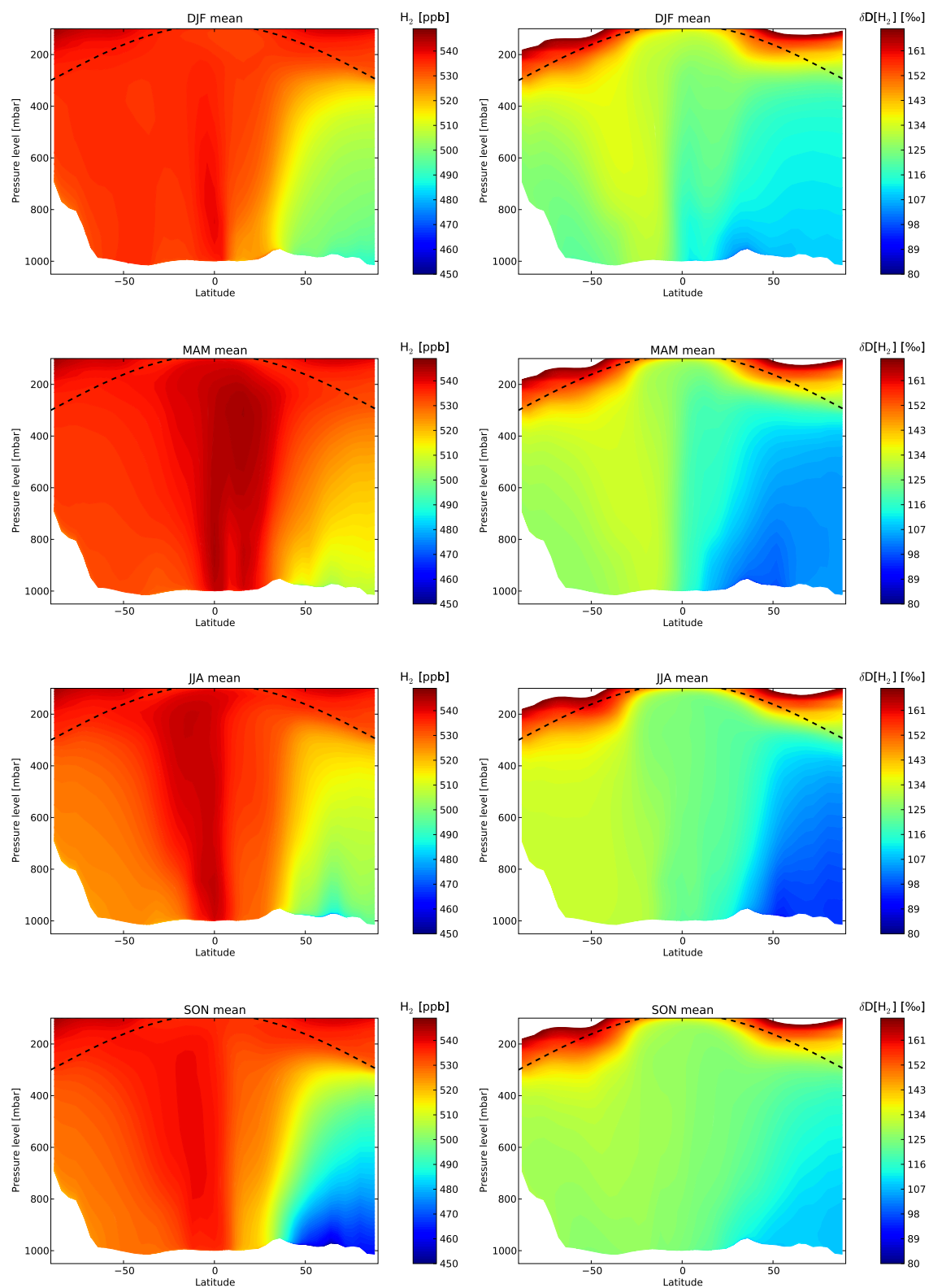


**Fig. 5.** Seasonal zonal mean  $\text{H}_2$  mixing ratio in ppb (left column) and isotopic composition in ‰ (right column) during the NH winter (DJF), spring (MAM), summer (JJA), and autumn (SON) season. The reference tropospheric boundary for the stratospheric parametrisation (see Sect. 2.3) is indicated by the dashed line.

isotopic composition. Interestingly, when a vertical gradient in  $\delta D[H_2]$  observed in the NH, it is opposite to what is expected from deposition. The fractionation in deposition leads to preferential removal of  $H_2$ , which would leave the atmosphere enriched in HD. However,  $\delta D[H_2]$  values near the surface are always lowest. Apparently, whereas deposition is clearly the driver for seasonality and vertical gradient of  $H_2$  mixing ratio in the NH, it has less effect on  $\delta D[H_2]$ . This is because the surface sources are strongly depleted in deuterium compared to the ambient reservoir, which overpowers the comparatively weak kinetic isotope effect in deposition. Surprisingly, on the seasonal scale, we again see an effect that is qualitatively in agreement with the fractionation expected from the sinks (mostly deposition, but some fraction of OH, see Batenburg et al., 2011). In SON, the  $H_2$  levels are lowest (due to depositional loss) and the  $\delta D[H_2]$  values are highest because HD remains preferentially in the atmosphere. So, deposition does affect the large-scale (temporal) evolution, but not the short-scale (vertical) distribution of  $\delta D[H_2]$ . It is noted however, that the inverse vertical gradient in the isotopic composition becomes less pronounced in the autumn season, when deposition reaches its maximum. This shows that deposition indeed leads to higher  $\delta D[H_2]$  values in the NH.

In the SH, the seasonality in isotopic composition appears to be driven by a varying input of  $H_2$  enriched in D subsiding from a pressure altitude of 300 mbar at  $50^\circ$  S down to the surface pressure level at  $20^\circ$  S. It is strongest during the NH winter (DJF) and spring season (MAM). The shape of this anomaly suggests a significant influence of stratosphere-troposphere exchange (STE) on the isotopic composition in the SH. Apparently, in the NH such a signal is almost completely attenuated by the surface sources. The role of STE will be addressed in more detail by the sensitivity studies in Sect. 3.6.

The seasonal mean surface level  $H_2$  mixing ratios are shown in the left column of Fig. 6. The most prominent feature is the well-established strong inter-hemispheric gradient. Whereas there is relatively little seasonal variability in the SH, the NH is characterised by large seasonal variability. Figure 6 also shows that  $H_2$  in the NH is strongly influenced by the landmasses. In the extratropics (mostly in the NH, but also in the SH), in general lower  $H_2$  mixing ratios are observed over land than over the ocean. This characteristic distribution is a consequence of the dominant role of the soil sink, which has the most prominent impact on the  $H_2$  mixing ratio during the autumn season (SON). In the Northern Hemisphere,  $H_2$  levels at certain locations can also be much higher than the ocean background. These signals are related to fossil fuel usage in the highly populated regions, or biomass burning in the tropics and near the borders between China and Siberia. These surface sources can produce strong  $H_2$  plumes that extend far over the ocean.

Looking at the isotopic composition (right column in Fig. 6) we can identify combustion processes by the clear

$\delta D[H_2]$  depletion. In particular the African and Asian tropical regions with high  $H_2$  mixing ratios and low isotopic composition are striking. Unfortunately, there are no data available to confirm these low  $\delta D[H_2]$  values, but the model captures the  $H_2$  measurements at the Tae-Ahn peninsula, Korea, well (see Fig. 2 in the previous section). Isotope measurements have been initiated to investigate whether  $\delta D[H_2]$  values  $<60\%$  actually occur. The precise  $\delta D[H_2]/H_2$  correlations should enable us to further constrain isotope source signatures in these regions.

On the global scale, the main  $\delta D[H_2]$  characteristic is the inter-hemispheric gradient. The seasonal cycle of  $\delta D[H_2]$  in the SH is much smaller than in the NH, similar to the mixing ratios. Interestingly, the seasonality in the NH shows a delay in its response to the seasonal cycle of deposition, resulting in a seasonal maximum during the northern hemispheric autumn (SON) and winter (DJF) season, which is further explained in Sect. 3.4.

### 3.4 Global $H_2$ budget and isotope budget

The TM5 model keeps track of the total budget of the different chemical tracers. Although no explicit budget is calculated for the troposphere, the tropospheric budget of  $H_2$  can be estimated from the budget up to 100 mbar in a similar way as presented by Sanderson et al. (2003) and Ehhalt and Rohrer (2009). The overall budget for  $H_2$  is shown in Table 1, along with other recently published budget estimates. The magnitudes of the photochemical and deposition budget terms for the  $H_2$  mixing ratio are in good agreement with the values reported by Novelli et al. (1999); Hauglustaine and Ehhalt (2002); Sanderson et al. (2003); Price et al. (2007); Ehhalt and Rohrer (2009); Yashiro et al. (2011). The values reported by Rhee et al. (2006) and Xiao et al. (2007) appear to be rather large compared to this and all other studies. The work by Ehhalt and Rohrer (2009) illustrates that the NMHC contribution to the production of  $H_2$  in the studies by Rhee et al. (2006); Xiao et al. (2007) is larger than can be reproduced by other full chemistry models that use bottom up estimates for NMHC emissions. Moreover, the study by Ehhalt and Rohrer (2009) provides an additional constraint via independent studies on carbon monoxide (CO) that narrows down the range for the total photochemical source of  $H_2$  to 40–46 Tg  $H_2$  yr<sup>-1</sup>. Recent TM5 model results for CO are also in good agreement with high frequency observations from several measurement sites in Europe (Pieterse et al., 2011). Hence, the reported values for the photochemical source magnitude between 30–41 Tg  $H_2$  yr<sup>-1</sup> appear to be more realistic than the values of 64 and 77 Tg  $H_2$  yr<sup>-1</sup> reported by Rhee et al. (2006) and Xiao et al. (2007). This also implies that the values for the removal by deposition between 55–60 Tg  $H_2$  yr<sup>-1</sup> and the reported tropospheric lifetimes around 2 yr are probably more realistic than the very large deposition fluxes and short turnover times proposed by Rhee et al. (2006) and Xiao et al. (2007).

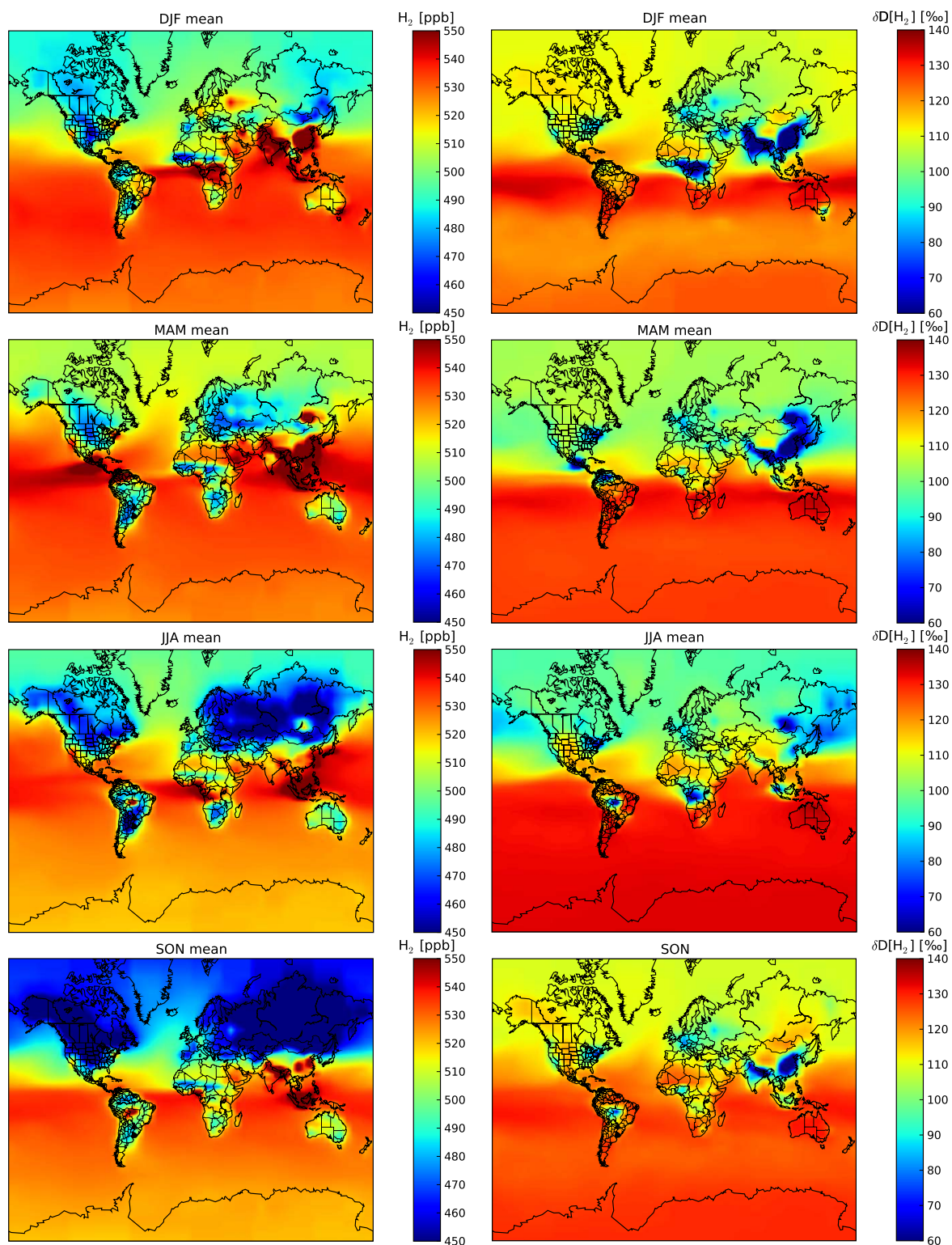


**Fig. 6.** Seasonal mean surface level  $\text{H}_2$  mixing ratio in ppb (left column) and isotopic composition in ‰ (right column) during the NH winter (DJF), spring (MAM), summer (JJA), and autumn (SON) season.

The H<sub>2</sub> isotope budget for the atmosphere up to 100 mbar is shown in Table 2. Because the H<sub>2</sub> and HD mixing ratios in the stratosphere are parametrised (see Sect. 2.3), the corresponding budget terms are bidirectional for both H<sub>2</sub> and HD and therefore not easily incorporated into the traditional isotope budget that only contains unidirectional source and sink terms. For the unidirectional terms, we can use the flux weighted ratios and fractionation constants to calculate the overall isotopic composition using the following expression (Gerst and Quay, 2001):

$$\delta D[\text{H}_2] = \frac{1}{R_{\text{VSMOW}}} \frac{\sum_i w_i R_i}{\sum_j w_j \alpha_j} - 1. \quad (6)$$

In this expression,  $R_i$  are the source isotope ratios and  $\alpha_j$  are the sink fractionation constants (see Table 2).  $w_i$  and  $w_j$  are the corresponding relative weights. This budget calculation yields an average isotopic composition of +99‰. The modelled average tropospheric composition obtained from the mixing ratio fields is +128‰. This means that a contribution of +29‰ can be inferred for the stratospheric contribution, a value similar to the value of +37‰ reported by Price et al. (2007).

The fractionation constants of the loss processes in Table 2 were obtained from the modelled H<sub>2</sub> and HD mixing ratios and fluxes by an approximation based on the Rayleigh distillation model for a single stage removal process  $j$  (Rayleigh, 1902):

$$\alpha_j \simeq \frac{L_{\text{HD},j} [\text{H}_2]_i}{L_{\text{H}_2,j} [\text{HD}]_i}, \quad (7)$$

where  $L_{\text{HD},j}$  and  $L_{\text{H}_2,j}$  are the overall removal fluxes.  $[\text{HD}]_i$  and  $[\text{H}_2]_i$  are the burdens for HD and H<sub>2</sub> at the start of the simulation. The resulting apparent fractionation for deposition (0.925) is stronger than the applied fractionation for the deposition (0.943) because the isotope composition of H<sub>2</sub> close to the surface is relatively light. This means that in Eq. (7), H<sub>2</sub>/HD at the surface where the removal fluxes are calculated is larger than H<sub>2</sub>/HD averaged over the entire atmosphere, the value used for the budget calculation. The photochemical source signature of +116‰ is at the low end, but within the ranges of +162<sup>+57</sup><sub>-57</sub>‰ and +130<sup>+70</sup><sub>-70</sub>‰ reported by Price et al. (2007) and Gerst and Quay (2001), respectively.

Also the global average isotopic composition of +128‰ seems to be well within the range of values reported by Gerst and Quay (2001); Rahn et al. (2002b); Rhee et al. (2006); Price et al. (2007), but it is noted that the region of the atmosphere up to 100 mbar includes a significant portion of stratospheric air at high latitudes. This results in an artificial enrichment in D of the tropospheric reservoir. Figure 3 in Sect. 3.2 already showed that the model underestimates the surface isotope measurements by approximately

10–20‰. Indeed, the budget for the lower troposphere (for pressure levels above 850 mbar) returns a value of +119‰. In Sect. 3.6 we will further investigate the sensitivity of the model results to changes in the parameters of the main processes in the H<sub>2</sub> cycle and identify the opportunities for changing these parameters to close the gap between the measurements and the model results.

### 3.5 Global variability in H<sub>2</sub> mixing ratios and isotopic compositions

In order to investigate the global scale variability in more detail, the monthly atmospheric burden and fluxes of H<sub>2</sub> and HD were integrated for three latitude bands, 90° S–30° S, 30° S–30° N, and 30° N–90° N, respectively. The height of the three top box boundaries was set to 100 mbar. Figure 7 shows the resulting seasonal cycles in the H<sub>2</sub> mixing ratio and isotopic composition in the three latitude bands.

This figure reproduces the established features of the global H<sub>2</sub> cycle, for example the large seasonal cycle in the H<sub>2</sub> mixing ratio in the Northern Hemisphere due to deposition (e.g., Novelli et al., 1999). To assess the variability in the mixing ratio and isotopic composition in the three different regions, all relevant processes should be considered, i.e. the emissions, photochemistry, deposition, horizontal advection, and vertical transport. We can analyse the H<sub>2</sub> isotope budget in the model in more detail by calculating the individual contribution of each source and sink process to the change of the H<sub>2</sub> mixing ratio and isotopic composition on the monthly basis. The mathematical framework is derived in Appendix C, and the results are shown in Fig. 8.

Starting from a certain mixing ratio and isotopic composition for a given month in Fig. 7, the mixing ratio and isotopic composition of the next month will be changed by an amount equal to the sum of the contributions shown in Fig. 8. For example, surface emissions (red bars in Fig. 8) always constitute a net source and show up as a positive bar for the mixing ratio. However, these surface emissions are strongly depleted in D compared to the ambient reservoir, and therefore lead to a decrease in the isotopic composition. In the model, these surface emissions have a strong seasonality in the extratropical boxes, but are rather constant in the tropics. Photochemical H<sub>2</sub> sources (green bars) can make a significant contribution to the total H<sub>2</sub> changes, especially in the tropics and the extratropical summer seasons, but the effect on the isotopic composition is negligible since the produced H<sub>2</sub> has an isotopic composition ( $\delta D[\text{H}_2] = 116\text{‰}$ ) very similar to the ambient reservoir.

The photochemical removal of H<sub>2</sub> at the higher NH latitudes shows up as a negative contribution to the monthly mixing ratio change (light blue bars in Fig. 8). Although the photochemical removal is relatively small in magnitude, it is associated with strong isotope fractionation, clearly visible as a strong positive contribution to the change in isotopic composition. Deposition (dark blue bars) is a stronger sink

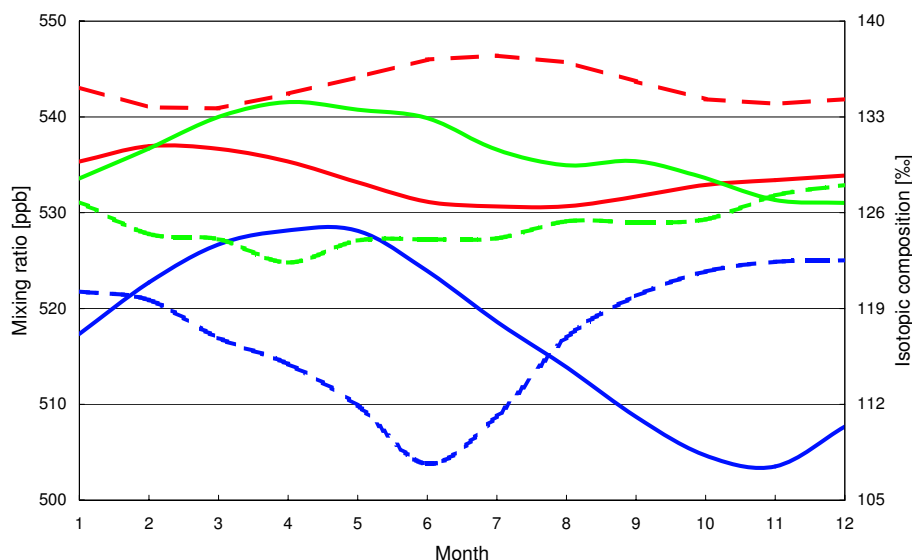


**Fig. 7.** The modelled seasonal cycle of the  $\text{H}_2$  mixing ratio (full lines) and isotopic composition (dashed lines) derived from the budgets of the latitude bands from (blue)  $90^\circ\text{N}$  to  $30^\circ\text{N}$ , (green)  $30^\circ\text{N}$  to  $30^\circ\text{S}$ , and (red)  $30^\circ\text{S}$  to  $90^\circ\text{S}$ .

than photochemical removal, but the effect on the isotopic composition is overall smaller, since the isotope fractionation constant in soil deposition is much closer to unity.

The final contributions are the horizontal flux (dark gray) and the stratospheric contribution (light gray). The former combines horizontal advection with the change of mass in each box due to the seasonal cycle in surface pressure (see Eq. (C2) in Appendix C). The stratospheric contribution also consists of two parts: the vertical exchange with air above the 100 mbar pressure level and the change in the correction provided by Eq. (2) and Eq. (4) above the boundary described by Eq. (1).

This alternative approach to investigate the variability in isotopic composition was stimulated by a peculiar property of the vertical and horizontal flux terms. Whereas the stratospheric contribution can be a sink for  $\text{H}_2$  in one month, it can become a source in the next. The same may occur for HD. This behaviour does not enable a budget analysis in the traditional way, i.e. describing sources with signatures in ‰ and describing sinks by fractionation constants. We can to some extent analyse the impact of the vertical exchange separately from the impact of the stratospheric parametrisation. The overall downward flux for the high-latitude boxes (HLBs) is  $5.8$  and  $7.2\text{ Tg yr}^{-1}$ , respectively for the Northern and Southern Hemisphere (with an average burden of  $41$  and  $42\text{ Tg}$  in the HLBs). Exchanging air in the NH and SH HLBs with an average composition of  $117$  ‰ and  $135$  ‰ (see Fig. 7) with stratospheric air with an estimated composition of  $180$  ‰ (see Fig. 5), coming from heights above 100 mbar, leads to an enrichment of  $9$  ‰ and  $7$  ‰, respectively. These values are comparable to the values of  $7$  ‰ and  $11$  ‰ presented by Rhee et al. (2006).

The budget analysis visualised in Fig. 8 allows a detailed attribution of the impact of the different processes on the variability of the mixing ratio and isotopic composition of  $\text{H}_2$ . The seasonal cycle of the isotopic composition in the higher northern latitudes is mainly determined by the seasonal cycle in the photochemical loss of  $\text{H}_2$ , deposition, and the surface emissions. As mentioned above, the photochemical source contributes has no “isotope leverage”, i.e. is not very different from the ambient reservoir, and only source processes with a significantly more enriched or depleted signature and sink processes will affect isotope variability. The seasonal cycle of the isotopic composition at higher northern latitudes (see Fig. 7) is slightly shifted due to the different seasonality of the surface emissions (fossil fuel using, biomass burning, and nitrogen fixation) compared to the seasonality of photochemistry and deposition. The small variability at tropical latitudes is mainly caused by slight variations in the surface emissions and the seasonal exchange with air masses from the Northern and Southern Hemispheres. The variability of the isotopic composition in the southernmost latitudes is mainly caused by seasonality in tropospheric photochemistry, counteracted by the surface emissions, and the exchange with  $\text{H}_2$  more depleted in D from the tropical latitudes from June to September. The vertical flux is an important term in the isotope budget of the southern latitudes during the winter season (JJA). Having identified the most important processes, we will investigate the sensitivity of the model to changes in the individual parameters in the next section.

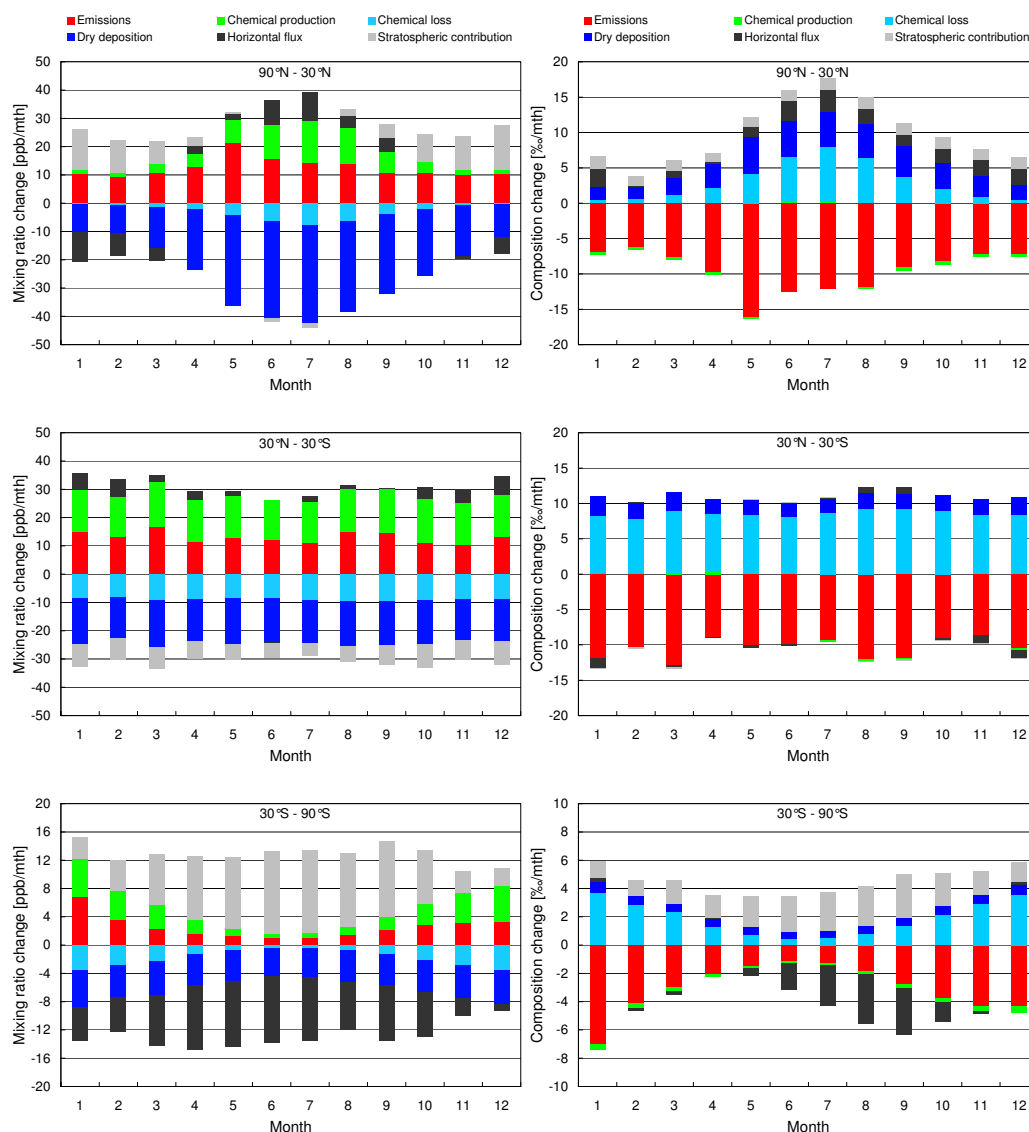


**Fig. 8.** The modelled contributions of the different processes to monthly changes in the mixing ratio (left column) and isotopic composition (right column) in Fig. 7, derived from the budgets of the latitude bands from 90° N to 30° N, 30° N to 30° S, and 30° S to 90° S.

### 3.6 Sensitivity study

The previous sections showed that the modelled isotopic composition has a small negative bias compared to the available measurements. Different options for closing the discrepancy between the model results and the measurements are available and viable. In this section, we will investigate the sensitivity of the modelled isotopic composition to changes in the key parameters of the molecular hydrogen isotope cycle whilst keeping the  $\text{H}_2$  budget unaltered.

In the methane and NMHC oxidation schemes, the final step towards the formation of  $\text{H}_2$  and HD, i.e. the destruction of formaldehyde ( $\text{CH}_2\text{O}$ ) is of large influence on the final isotopic composition (Feilberg et al., 2007a; Pieterse et al.,

2009). Therefore the sensitivity of the isotopic composition to changing the KIEs of the molecular and radical pathway of the two photolysis reactions of  $\text{CH}_2\text{O}$  was examined first. Case 1a (Table 3) employs the KIEs reported by Feilberg et al. (2007a). Evidently, the isotopic composition is very sensitive to changes in the KIEs for formaldehyde photolysis. As noted in Pieterse et al. (2009), the KIEs for the radical (R32b) and molecular (R33) photolysis removal channels for formaldehyde used for this case lead to a strong underestimation of the isotopic composition and a photochemical source signature of  $-87\%$ .

In case 1b, the sensitivity of the isotopic composition to changes in the pressure dependency of the KIE of Reaction (R33b) (see Eq. (A4) in Appendix A4) is investigated.

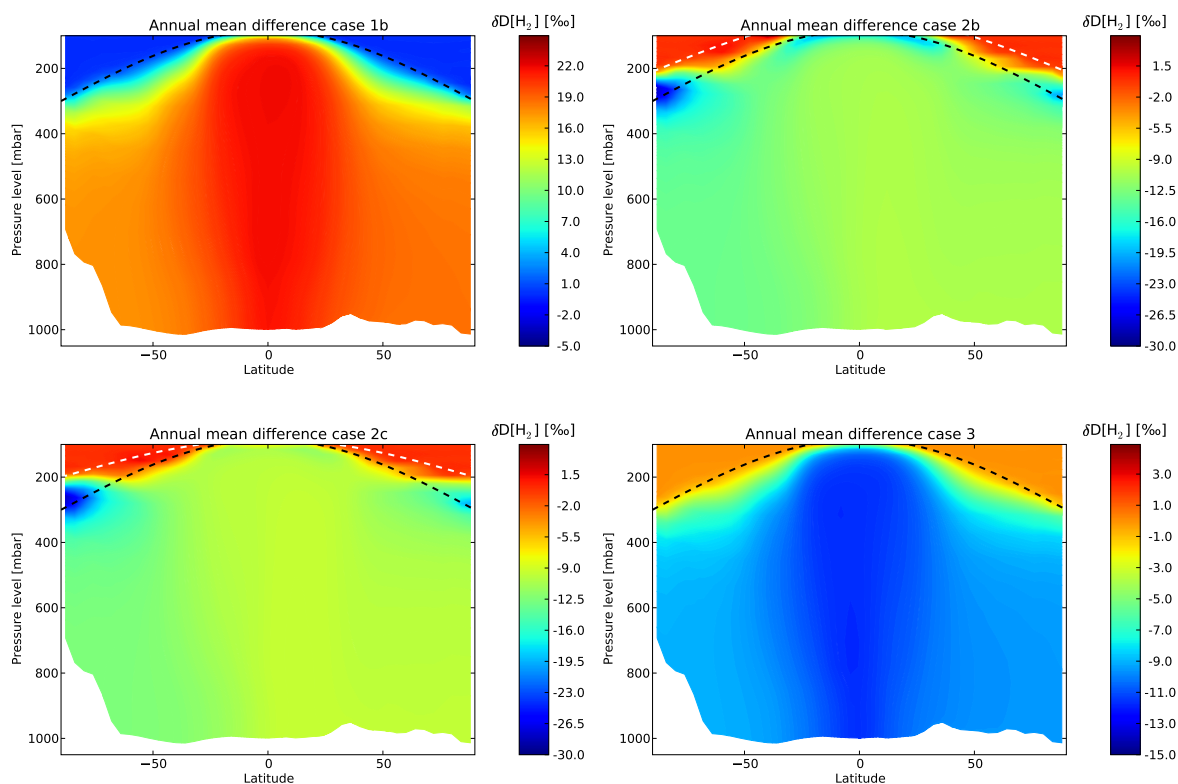


**Fig. 9.** Zonal annual mean differences for case 1b, case 2b, case 2c, and case 3. The reference tropospheric boundary for the stratospheric parametrisation (see Sect. 2.3) is indicated by the dashed black line. The perturbed boundaries of case 2b and 2c are indicated by the dashed white line.

**Table 3.** Sensitivity of isotopic composition of H<sub>2</sub> on changes in parameters of the isotope scheme.

Scenario	Perturbed variables	Composition (‰)
Reference <sup>a</sup>		+128
1a	KIE[R32b] = 1.100, KIE[R33b] = 1.820	+82
1b	$KIE[R33b] = (500.00 + 2.50 \times 10^{-2} p) / (500.00 + 1.60 \times 10^{-2} p)$	+146
2a	Stratospheric composition increased by 20 ‰	+140
2b	Tropopause boundary defined by $p_s = 2.10 \times 10^4 - 1.65 \times 10^4 \cos(\theta)$	+116
2c	Tropopause boundary defined by $p_s = 2.00 \times 10^4 - 1.15 \times 10^4 \cos(\theta)$	+118
3	$\delta D[\text{NMHCs}] = -200 \text{ ‰}$	+118
4a	$\delta D[\text{N}_2 \text{ fixation emissions}] = -700 \text{ ‰}$	+124
4b	$\delta D[\text{fossil fuel burning emissions}] = -250 \text{ ‰}$	+123
4c	$\delta D[\text{biomass burning emissions}] = -290 \text{ ‰}$	+125
5	Fractionation constant deposition changed to 0.900	+142

<sup>a</sup> The reference scenario uses KIE[R32b] = 1.580, KIE[R33b] =  $(500.00 + 2.50 \times 10^{-2} p) / (500.00 + 1.34 \times 10^{-2} p)$ , a tropopause composition of +130 ‰, a tropopause boundary defined by  $p_s = 3.00 \times 10^4 - 2.15 \times 10^4 \cos(\theta)$ ,  $\delta D[\text{NMHCs}] = -86 \text{ ‰}$ ,  $\delta D[\text{N}_2 \text{ fixation emissions}] = -628 \text{ ‰}$ ,  $\delta D[\text{fossil fuel burning emissions}] = -196 \text{ ‰}$ ,  $\delta D[\text{biomass burning emissions}] = -260 \text{ ‰}$ , and fractionation constant of 0.943 for deposition.

Changing this parameter clearly leads to a large increase in isotopic composition of 18 ‰ and a photochemical source signature of +199 ‰. As expected, the tropospheric composition is very sensitive to changes in the pressure dependency of the molecular photolysis removal channel for formaldehyde, especially in the tropics, as shown in the zonal annual mean difference plot in Fig. 9.

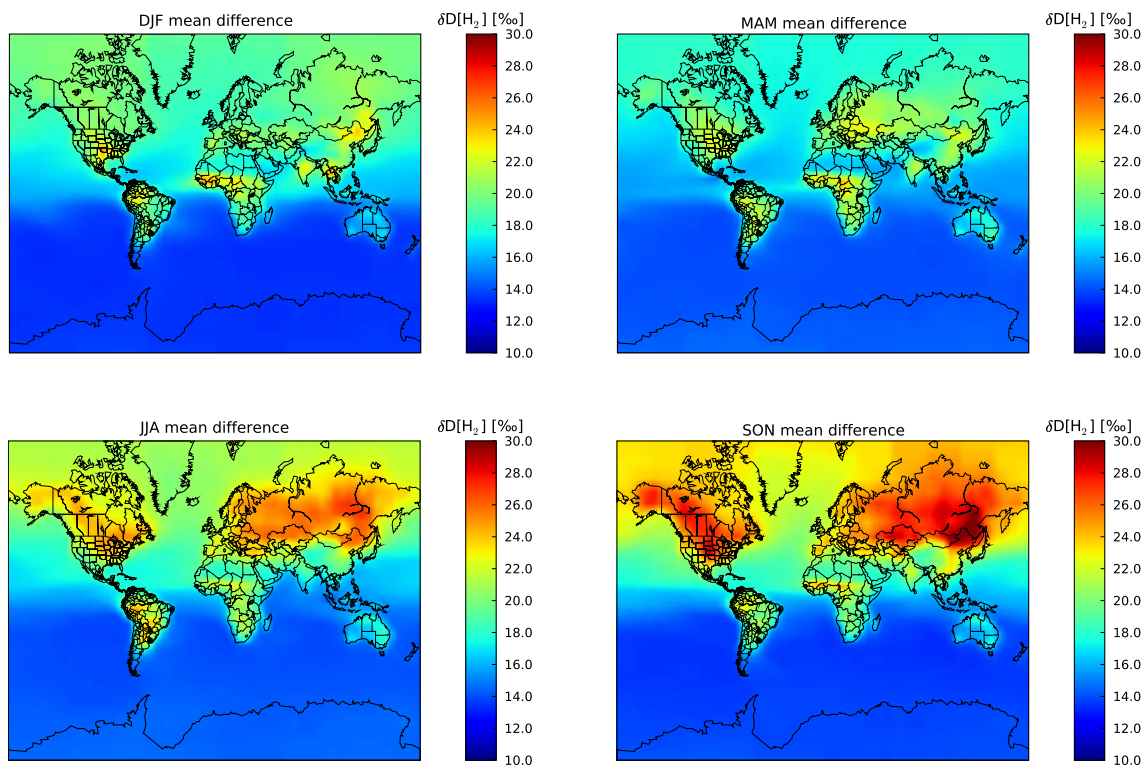
The sensitivity of the tropospheric composition to changes in the stratospheric parametrisation was tested by increasing the isotopic composition in the stratosphere by 20 ‰ compared to the reference scenario (case 2a). The effect on the average tropospheric value of  $\delta D[H_2]$  is profound (an increase of 12 ‰).  $H_2$  produced in the stratosphere is highly enriched in D (Rahn et al., 2003; Röckmann et al., 2003; Mar et al., 2007). Therefore, the back-flux of stratospheric hydrogen can significantly enrich  $H_2$  in the troposphere, as was already concluded from the results in Table 2 and Fig. 8 in Sect. 3.4. The sensitivity of the model to changes in the stratospheric parametrisation was further investigated by changing Eq. (1) in Sect. 2.3 (case 2b and 2c). The cases were carefully chosen to distinguish between (2b) STE at higher latitudes and (2c) STE near the tropical tropopause layer (TTL). Both cases show that the isotopic composition is also sensitive to changes in the pressure levels above which the parametrisation described in Sect. 2.3 is used. Changes near the TTL were not expected to affect tropospheric composition because  $H_2$  is photochemically produced in this region and then transported upwards into the stratosphere. Indeed, the results of case 2b and 2c show similar small effects on the tropospheric isotopic composition, both in magnitude and distribution (see Fig. 9). Thus,  $H_2$  strongly enriched in D is injected from the mid-latitude stratosphere into the troposphere (e.g., Reid and Vaughan, 1991; Appenzeller et al., 1996; Lelieveld et al., 1997; Hintsä et al., 1998; Dethof et al., 2000). This effect is also clearly visible in the zonal mean isotopic composition during the NH winter and spring season shown in Fig. 5, and is more pronounced in the SH because in the NH it is damped by the seasonality in the surface emissions (see Fig. 8) resulting in less enrichment.

Figure 3 shows that increasing the isotopic composition at and above the tropopause by 20 ‰ closes the gap between the reference scenario isotopic composition and the observations. It is noted however that previous studies have shown that the Brewer-Dobson circulation is overestimated by the meteorological data from ECMWF and consequently the downward transport from the stratosphere to the troposphere is a factor 2–3 too high, at least for ozone (van Noije et al., 2004, 2006). This could mean that the actual downward transport of heavy hydrogen (i.e. the contribution to the isotope budget) might be significantly lower than predicted by the TM5 model. However, the effect of the stratosphere on the tropospheric isotopic composition of  $H_2$  was also observed by Price et al. (2007) who used another global chemical transport model (CTM) driven by a different meteorology; The stratospheric contribution to the tropospheric iso-

topic composition computed in the current study (+29 ‰) is similar to their calculated contribution of +37 ‰, calculated using the GEOS-chem CTM. Thus, the results of both models suggest that STE is a potentially important process for the tropospheric isotope budget of  $H_2$ . Measuring the isotopic composition at the tropopause and in the lower stratosphere is therefore important to refine the upper boundary condition for the tropospheric model simulations.

Case 3 was chosen to investigate the sensitivity of the model results to the initial isotopic compositions of the NMHCs participating in the  $H_2$  cycle. The full NMHC hydrogen isotope chemistry mechanism consists of a large set of chemical reactions and is poorly constrained by available measurements. We believe that with so many unverified parameters, a comprehensive sensitivity study of the mechanism would not be of value at this time. Therefore, we chose to test the sensitivity of the isotopic composition to changes in the initial isotopic composition from –86 ‰ to –200 ‰. The result (a decrease of 10 ‰) in Table 3 shows that the model is indeed sensitive to changing the isotopic composition of the NMHCs, although it is noted that the applied perturbation was large (a decrease of 114 ‰) and the effect is relatively small (see Fig. 9).

In the fourth set of cases, the sensitivity of the model output on the isotopic composition of the surface sources is investigated. For case 4a, we implemented an isotopic source signature of –700 ‰ for terrestrial and oceanic nitrogen fixation processes. This value is similar to new measurements on biologically produced  $H_2$  (Walter et al., 2011), which agree with calculations on the thermodynamic isotope equilibrium between  $H_2$  and  $H_2O$  (Rahn et al., 2003). The simulated change in  $\delta D[H_2]$  compared to the reference scenario given in Table 3 is small, as was to be expected from the isotope budget shown in Table 2. Hence, the model results are not very sensitive to changes in the isotopic composition of biologically produced  $H_2$ . For case 4b, the isotopic source signature of the fossil fuel sources was decreased to –250 ‰. The new value is the average of the values for incomplete and full catalytic conversion of exhaust fumes, recently reported by Vollmer et al. (2010). The difference will be only noticeable in highly populated areas where fossil fuel usage is an important source. On the global scale, however, the isotopic composition is barely affected by the change in the isotope source signature. The sensitivity of the model results to a change in the isotopic signature of the biomass burning emissions to the value suggested by Gerst and Quay (2001) was tested in case 4c. Again, the global average change in  $\delta D[H_2]$  due to a change in the source signature of  $H_2$  from biomass burning relative to the reference scenario is small. Thus, all sub-scenarios of case 4, which explore the previously reported ranges of uncertainty in the source signatures, do not lead to a strong change in global average  $\delta D[H_2]$  values. This implies that the available surface source signatures are sufficiently constrained to close the global  $H_2$  isotope budget, although more accurate values might be required to



**Fig. 10.** Case 5 surface level seasonal mean difference.

close the regional budgets. For example, it has been demonstrated recently that the isotopic composition of  $H_2$  emitted from biomass burning is closely related to the  $\delta D$  value of the local precipitation (Röckmann et al., 2010b), which can vary spatially by more than 100 ‰. This should be considered in future model studies where regional impact of biomass burning is expected.

With case 5, the sensitivity of the model to changes in the fractionation constant for deposition from 0.943 to 0.900 was investigated (see Fig. 10). This is outside the reported range of  $\pm 1\sigma$  uncertainty of  $0.943 \pm 0.024$  (Gerst and Quay, 2001), but unpublished data (Rahn et al., 2005) indicate that, depending on ecosystem type and season, fractionation constants as low as 0.900 can be observed. The regional isotope budgets, especially above the Eurasian continent, are very sensitive to small changes in the fractionation associated with deposition. This is thus an important model parameter that should be tested in more detail experimentally.

In conclusion, three cases provide good opportunities to reduce the bias between the modelled and measured gradient. Case 1b shows that implementing a different pressure sensitivity of R33 could solve the bias between the modelled and measured global isotopic composition. Also, an increase of 20 ‰ in the isotopic composition at the tropopause (case 2a) could suffice. Finally, case 5 reduces the difference by employing a lower fractionation constant for deposition (0.900 in stead of 0.943). It is clear that the parameters of case 1b

and 5 were perturbed outside the reported ranges of uncertainty. Nevertheless, a combination of changes within range of uncertainty of the involved parameters can resolve the bias between the modelled and measured isotopic composition (see Fig. 3 in Sect. 3.2). Another way to try to close the isotope budget is to implement photochemical NMHC sources of  $H_2$  that are not yet considered in the TM5 model, e.g. the methanol emissions or the chemistry of the monoterpenes. These options were not considered here because exploratory budget calculations showed that this would not close the gap between the measurements and the model results.

#### 4 Conclusions

We have implemented  $H_2$  sources and sinks, including isotopic composition, and a simplified but explicit isotope photochemistry scheme into the TM5 global chemistry transport model. On the seasonal and inter-annual time scale, the modelled mixing ratios were found to be in good agreement with all observations. The global budget also showed that the model adequately reproduces the established values for the tropospheric burden and atmospheric lifetime of  $H_2$  (155 Tg  $H_2$  and 2.0 yr, respectively). In all, the model provides a very adequate description of the global  $H_2$  cycle.

Regarding the isotopic composition, the mean zonal gradient of the modelled surface isotopic composition shows

a consistent negative bias of approximately 10–20%. The uncertainties in the relevant parameters of the isotope model are significant and provide room for adjustments within the ranges of uncertainty without changing the source and sink magnitudes. However, the observed latitudinal gradient in the isotopic composition constrains the possibilities of closing the H<sub>2</sub> isotope budget on a global scale to a limited number of parameters. For example, reducing the fractionation constant for deposition has a larger impact on the isotopic composition in the NH than in the SH. Thus, this change tends to reduce the inter hemispheric gradient.

Exchange with the stratosphere has a strong influence on the isotopic composition of H<sub>2</sub> in the troposphere. As tracers like Cl and O(<sup>1</sup>D) are not implemented in the CBM-4 scheme, stratospheric chemistry is not accurately represented in TM5. Therefore, the isotopic composition of H<sub>2</sub> in the stratosphere is parametrised following empirical correlations (McCarthy et al., 2004). The parametrisation for tropopause height used here is rather crude, but the model results prove to be robust within a few ‰ to significant changes in the imposed tropopause height. This is because the model tropopause was defined at a height above the region where STE takes place. The actual isotopic composition above the model tropopause boundary appears a much stronger driver. Although the STE flux of H<sub>2</sub> is small in magnitude compared to other fluxes that affect the tropospheric H<sub>2</sub> isotope budget, its source signature is significantly enriched. It is noted that STE is probably overestimated because the ECMWF model is known to have a too fast Brewer-Dobson stratospheric circulation due to its relatively coarse vertical resolution. Hence, the impact of the STE on the tropospheric isotopic composition may be too large as well. However, our estimate of 29 ‰ for the stratospheric contribution is similar to the value of 37 ‰ found in Price et al. (2007), even though different meteorological data are used to drive the vertical transport in the two models. Given that both models use the parametrisation based on McCarthy et al. (2004), their results might be similarly affected by shortcomings in this parametrisation, if any. Nonetheless, STE appears a relevant subject for future studies of the tropospheric isotope budget of H<sub>2</sub>. Tropospheric surface measurements of the isotopic composition will not discern between H<sub>2</sub> photochemically produced in the troposphere or the stratosphere. Thus, the significance of the stratospheric impact might pass unnoticed.

As the isotopic composition is calculated including a full isotope chemistry scheme, it is also possible to study the isotope budgets of chemical precursors. We consider the isotope budget of formaldehyde (CH<sub>2</sub>O) as an important tool to evaluate the impact of the different photochemical processes on the final isotopic composition of H<sub>2</sub>, and to improve the model if measurements at sufficient precision become available. In the present situation, the available isotope data do not provide sufficient information to independently constrain the global isotope budget. Additional studies focussing on

the isotope effects in the photochemistry and deposition in non background conditions as well as isotope measurements near the tropopause are therefore recommended.

## Appendix A

### Derivation of the methane reaction mechanism

The new methane related reactions implemented in the TM5 model are shown in Table A1. To enable unambiguous reference to the original CBM-4 scheme (Houweling et al., 1998), we chose to use the original reaction numbering. Methane background mixing ratio fields obtained using the four-dimensional variational (4-D-Var) data assimilation system implemented in TM5 (Meirink et al., 2008a,b) are used to prescribe the CH<sub>4</sub> mixing ratio fields. The mixing ratios of the singly deuterated methane isotopologue (CH<sub>3</sub>D) are fixed by asserting a uniform isotopic composition of –86 ‰ for the entire atmosphere, which is justified because the observed atmospheric variability is small (Quay et al., 1999), neglecting spatial and temporal variability.

Budget calculations with the TM5 model configuration presented in this work yield an estimated atmospheric lifetime of 8.3 yr, when accounting for the non-modelled loss by Cl and O(<sup>1</sup>D). This value is in good agreement with the value of 8.4 yr reported by Houghton et al. (2001) and implies realistic values for the mixing ratios of the hydroxyl radical (OH) that also removes H<sub>2</sub> and HD.

#### A1 Reaction of methane (CH<sub>4</sub>)

The KIE of the reaction of the methane isotopologues (R26a and R26b) directly follows from the recommendations in Sander et al. (2006). The branching ratio was calculated following the method discussed previously by Pieterse et al. (2009).

$$\alpha_{\text{CH}_3\text{D}+\text{OH}}^{\text{D}} = \frac{3}{4} \text{KIE}_{\text{CH}_4+\text{OH}}. \quad (\text{A1})$$

In this reaction, KIE<sub>CH<sub>4</sub>+OH</sub> is calculated as the ratio between the rate coefficient of the deuterated and the non deuterated methane isotopologue. Because this ratio is temperature dependent, the branching ratio is also temperature dependent and therefore it is calculated online. TM5 does not consider the intermediate methyl radical CH<sub>3</sub> and immediately forms the methylperoxy radical (CH<sub>3</sub>OO) via O<sub>2</sub> addition, as described for example in Ravishankara (1988). It is assumed that isotope effects in this fast intermediate reaction are negligible.

#### A2 Reactions of the methylperoxy radical (CH<sub>3</sub>O<sub>2</sub>)

The reaction of CH<sub>3</sub>OO with nitric oxide (NO) forms the methoxy radical (CH<sub>3</sub>O). A possible hydrogen isotope effect in this reaction will likely be very small since hydrogen

**Table A1.** Overview of modified CBM-4 reactions related to methane and molecular hydrogen chemistry.

Number	Reaction	A	−E/R	<i>n</i>	KIE	Reference
R21a	H <sub>2</sub> + OH → HO <sub>2</sub>	2.8 × 10 <sup>−12</sup>	−1800			JPL06
R21b	HD + OH → <sup>a</sup>	5.0 × 10 <sup>−12</sup>	−2130			JPL06
R26a	CH <sub>4</sub> + OH → CH <sub>3</sub> OO	2.45 × 10 <sup>−12</sup>	−1775			JPL06
R26b	CH <sub>3</sub> D + OH → <sup>a</sup> <sub>D</sub> CH <sub>2</sub> DOO	3.50 × 10 <sup>−12</sup>	−1950			JPL06
R27a	CH <sub>3</sub> OO + NO → CH <sub>2</sub> O + HO <sub>2</sub> + NO <sub>2</sub>	4.2 × 10 <sup>−12</sup>	180			JPL
R27b	CH <sub>2</sub> DOO + NO → 0.882CHDO <sup>a</sup>				1.323	GP
R28a	CH <sub>3</sub> OO + HO <sub>2</sub> → CH <sub>3</sub> OOH	3.8 × 10 <sup>−13</sup>	800			JPL
R28b	CH <sub>2</sub> DOO + HO <sub>2</sub> → CH <sub>2</sub> DOOH				1.000	GP
R29a	CH <sub>3</sub> OO + CH <sub>3</sub> OO → 2.000CH <sub>2</sub> O + 0.667HO <sub>2</sub>	2.5 × 10 <sup>−13</sup>	190			JPL
R29b	CH <sub>2</sub> DOO + CH <sub>3</sub> OO → 0.810CHDO <sup>a</sup>				1.221	<sup>b</sup>
R30a	CH <sub>3</sub> OOH + OH → 0.700CH <sub>3</sub> OO + 0.300CH <sub>2</sub> O + 0.300OH	3.8 × 10 <sup>−12</sup>	200			JPL
R30b	CH <sub>2</sub> DOOH + OH → 0.755CH <sub>2</sub> DOO + 0.216CHDO <sup>a</sup>				1.079	GP
R31a	CH <sub>3</sub> OOH $\xrightarrow{h\nu}$ CH <sub>2</sub> O + HO <sub>2</sub> + OH					BC
R31b	CH <sub>2</sub> DOOH $\xrightarrow{h\nu}$ 0.882CHDO <sup>a</sup>				1.323	GP
R32a	CH <sub>2</sub> O $\xrightarrow{h\nu}$ 2HO <sub>2</sub> + CO					BC
R32b	CHDO $\xrightarrow{h\nu}$ <sup>a</sup>				1.580	BC
R33a	CH <sub>2</sub> O $\xrightarrow{h\nu}$ CO + H <sub>2</sub>					MO
R33b	CHDO $\xrightarrow{h\nu}$ CO + HD				<sup>c</sup>	
R34a	CH <sub>2</sub> O + OH → HO <sub>2</sub> + CO	5.5 × 10 <sup>−12</sup>	125			JPL06
R34b	CHDO + OH → <sup>a</sup>				1.280	<sup>d</sup>
R35a	CH <sub>2</sub> O + NO <sub>3</sub> → HNO <sub>3</sub> + HO <sub>2</sub> + CO	5.8 × 10 <sup>−16</sup>				AT1
R35b	CHDO + NO <sub>3</sub> → <sup>a</sup>				1.000	<sup>e</sup>

In this table, the rate constants are in molec<sup>*p*</sup> cm<sup>−*q*</sup> s<sup>−1</sup>, with *p* and *q* reaction molecularity dependent. Photolysis rates are wavelength and intensity dependent (see references). CO<sub>2</sub>, O<sub>2</sub> and H<sub>2</sub>O are not listed in reaction products. BC, Brühl and Crutzen (1992); GP, Pieterse et al. (2009); JPL, DeMore et al. (1994); JPL06, Sander et al. (2006); MO, Moortgat et al. (1980); AT, Atkinson et al. (1992).

<sup>a</sup> The production of the deuterium free radical species is neglected because of the small amount of the deuterium containing precursor compared to the deuterium free precursor.

<sup>b</sup> Derived in Sect. A2.

<sup>c</sup> Here KIE = (500.00 + 2.50 × 10<sup>−2</sup> *p*) / (500.00 + 1.34 × 10<sup>−2</sup> *p*), where *p* is the ambient pressure in Pa (Nilsson et al., 2010; Röckmann et al., 2010a).

<sup>d</sup> Derived in Sect. A4.

<sup>e</sup> Because this term is of little importance for the H<sub>2</sub> budget, isotope effects are not considered here.

atoms are not directly involved, therefore it is neglected. The reaction of the methoxy radical with O<sub>2</sub> forms formaldehyde (CH<sub>2</sub>O). This hydrogen abstraction reaction has a strong KIE of 1.323 (Nilsson et al., 2007) and a significant isotopic branching (IB) ratio, i.e. 0.882, which strongly affect the isotopic composition of formaldehyde (CH<sub>2</sub>O). In the TM5 model, the methoxy radical is not implemented and the sequence of the two elementary reactions is condensed into Reaction (R27). In the absence of temperature dependent data at the time of this study, the KIE and IB ratio are assumed constant for the entire atmosphere.

The methylperoxy radical also combines with the hydroperoxy radical (HO<sub>2</sub>), via Reaction (R28). Because the hydrogen atom of HO<sub>2</sub> is added to the peroxy group, and the deuterium in the methyl group of CH<sub>3</sub>OO is not directly involved in the formation of methyl hydroperoxide (CH<sub>3</sub>O<sub>2</sub>H), the KIE and IB ratio are set equal to unity.

The last removal mechanism of CH<sub>3</sub>OO that is implemented in TM5 is its self Reaction (R29). Although the isotope effects in the primary reaction are very likely small, there are several subsequent reactions via methanol (CH<sub>3</sub>OH) for which isotope effects must be considered (DeMore et al., 1994; Sander et al., 2006; Pieterse et al., 2009). The fraction of deuterons that ends up in the final reservoir species formaldehyde is not straightforward to calculate. Pieterse et al. (2009) implemented the intermediate steps following the initial self reaction, shown in Table A2.

Using the IB ratios and KIEs in this table (also derived by Pieterse et al., 2009), the overall KIE and IB ratio for Reaction (R29b) in Table A1 are calculated as follows:

**Table A2.** Reactions following the CH<sub>3</sub>OO self reaction (Sander et al., 2006; Pieterse et al., 2009).

Number	Reaction	IB ratio	KIE
B1a <sub>1</sub>	CH <sub>3</sub> OO + CH <sub>3</sub> OO	$\xrightarrow{0.333}$	2CH <sub>3</sub> O + O <sub>2</sub>
B1a <sub>2</sub>		$\xrightarrow{0.667}$	CH <sub>3</sub> OH + CH <sub>2</sub> O + O <sub>2</sub>
B1b <sub>1</sub>	CH <sub>2</sub> DOO + CH <sub>3</sub> OO	$\xrightarrow{0.333}$	CH <sub>2</sub> DO + CH <sub>3</sub> O + O <sub>2</sub> 1.000
B1b <sub>2</sub>		$\xrightarrow{0.334}$	CH <sub>2</sub> DOH + CH <sub>2</sub> O + O <sub>2</sub> 1.000
B1b <sub>3</sub>		$\xrightarrow{0.222}$	CH <sub>3</sub> OH + CHDO + O <sub>2</sub> 1.000
B1b <sub>4</sub>		$\xrightarrow{0.111}$	CH <sub>3</sub> OD + CH <sub>2</sub> O + O <sub>2</sub> 1.000
B2a <sub>1</sub>	CH <sub>3</sub> OH + O <sub>2</sub>	$\xrightarrow{0.150}$	CH <sub>3</sub> O + H <sub>2</sub> O
B2a <sub>2</sub>		$\xrightarrow{0.850}$	CH <sub>2</sub> OH + H <sub>2</sub> O
B2b <sub>1</sub>	CH <sub>2</sub> DOH + OH	$\xrightarrow{0.189}$	CH <sub>2</sub> DO + H <sub>2</sub> O 1.262
B2b <sub>2</sub>		$\xrightarrow{0.715}$	CHDOH + H <sub>2</sub> O 1.262
B2b <sub>3</sub>		$\xrightarrow{0.096}$	CH <sub>2</sub> OH + HDO 1.262
B2c <sub>1</sub>	CH <sub>3</sub> OD + OH	$\xrightarrow{1.000}$	CH <sub>2</sub> OD + H <sub>2</sub> O 1.176
B2c <sub>2</sub>		$\xrightarrow{0.000}$	CH <sub>3</sub> O + HDO 1.176
B3a	CH <sub>2</sub> OH + O <sub>2</sub>	$\xrightarrow{1.000}$	CH <sub>2</sub> O + HO <sub>2</sub>
B3b	CH <sub>2</sub> OD + O <sub>2</sub>	$\xrightarrow{1.000}$	CH <sub>2</sub> O + DO <sub>2</sub> 1.000
B3c	CHDOH + O <sub>2</sub>	$\xrightarrow{1.000}$	CHDO + HO <sub>2</sub> 1.000
B4a	CH <sub>3</sub> O + O <sub>2</sub>	$\xrightarrow{1.000}$	CH <sub>2</sub> O + HO <sub>2</sub>
B4b <sub>1</sub>	CH <sub>2</sub> DO + O <sub>2</sub>	$\xrightarrow{0.882}$	CHDO + HO <sub>2</sub> 1.323
B4b <sub>2</sub>		$\xrightarrow{0.118}$	CH <sub>2</sub> O + DO <sub>2</sub> 1.323

$$\text{IB} = \text{IB}[\text{B1b}_1] \cdot \text{IB}[\text{B4b}_1] + \text{IB}[\text{B1b}_2] \cdot (\text{IB}[\text{B2b}_1] \cdot \text{IB}[\text{B4b}_1] + \text{IB}[\text{B2b}_2] \cdot \text{IB}[\text{B3c}]) = 0.810, \quad (\text{A2})$$

and:

$$\begin{aligned} \text{KIE} &= \text{KIE}[\text{B1b}] \cdot \text{IB}[\text{B1b}_1] \cdot \text{KIE}[\text{B4b}] + \\ &\quad \text{KIE}[\text{B1b}] \cdot \text{IB}[\text{B1b}_2] \cdot \text{KIE}[\text{B2b}] \cdot (\text{IB}[\text{B2b}_1] \cdot \\ &\quad \text{KIE}[\text{B4b}] + \text{IB}[\text{B2b}_2] \cdot \text{KIE}[\text{B3c}]) + \\ &\quad \text{KIE}[\text{B1b}] \cdot \text{IB}[\text{B1b}_3] \\ &= 1.221. \end{aligned} \quad (\text{A3})$$

### A3 Reactions of methyl hydroperoxide (CH<sub>3</sub>O<sub>2</sub>H)

Methyl hydroperoxide is oxidised with OH (R30) via two channels, one forming a CH<sub>3</sub>OO radical and the other forming a CH<sub>2</sub>O<sub>2</sub>H radical that immediately dissociates to formaldehyde. The photochemical destruction of methyl hydroperoxide produces CH<sub>3</sub>O that reacts to formaldehyde with oxygen. The values for the IB ratios and the KIE for these two reactions were taken from Pieterse et al. (2009).

### A4 Reactions of formaldehyde (CH<sub>2</sub>O)

The removal reactions of formaldehyde are the most crucial for correct hydrogen isotope modelling (Feilberg et al., 2007a; Rhee et al., 2008; Pieterse et al., 2009; Nilsson et al., 2010; Röckmann et al., 2010a). In the study by Feilberg et al. (2007a) an overall KIE for the photolysis of 1.58 was found, and values of 1.82 and 1.10 were reported for the molecular channel and radical channel, respectively. However, the exact isotope effects in the two individual photolysis reactions (R32 and R33) are still subject of discussion (Pieterse et al., 2009; Röckmann et al., 2010a). The reported KIEs lead to a significant mismatch between the actual relative magnitudes of the two photochemical pathways when matched to the overall KIE. New experimental data suggest that the KIE of the molecular channel is pressure dependent:

$$\text{KIE} = \frac{500.00 + 2.50 \times 10^{-2} p}{500.00 + 1.34 \times 10^{-2} p}, \quad (\text{A4})$$

with the pressure  $p$  in Pa (Nilsson et al., 2010) where the parameters have been adjusted to a value of 1.63 at atmospheric pressure (Röckmann et al., 2010a). These data also suggest that the KIE of the radical channel should be much closer to the KIE of the molecular channel than postulated by

**Table B1.** Overview of modified CBM-IV NMHC reactions.

Number	Reaction		A	-E/R	<i>n</i>	KIE	Reference
R37	ALD2 + OH	→	HO <sub>2</sub>				G1
R38a	ALD2 + NO <sub>3</sub>	→	C <sub>2</sub> O <sub>3</sub> + HNO <sub>3</sub>				G1
R38b	ALD2(D) + NO <sub>3</sub>	→	<sup>a</sup>			1.000	<sup>b</sup>
R39a	ALD2	$\xrightarrow{h\nu}$	CH <sub>2</sub> O + XO <sub>2</sub> + CO + 2HO <sub>2</sub>				LS
R39b	ALD2(D)	$\xrightarrow{h\nu}$	CHDO <sup>c</sup>			1.000	<sup>b</sup>
R40a	C <sub>2</sub> O <sub>3</sub> + NO	→	CH <sub>3</sub> O <sub>2</sub> + NO <sub>2</sub>				G2
R40b	C <sub>2</sub> O <sub>3</sub> (D) + NO	→	CH <sub>2</sub> DO <sub>2</sub> (D) <sup>c</sup>			1.000	<sup>b</sup>
R41	C <sub>2</sub> O <sub>3</sub> + NO <sub>2</sub>	$\xrightarrow{M}$	PAN				ATG
			<i>k</i> <sub>0</sub>			-7.1	
			<i>k</i> <sub>∞</sub>			0.9	
R42	PAN	→	C <sub>2</sub> O <sub>3</sub> + NO <sub>2</sub>				G2
R43	PAN	$\xrightarrow{h\nu}$	C <sub>2</sub> O <sub>3</sub> + NO <sub>2</sub>				SEN
R44a	C <sub>2</sub> O <sub>3</sub> + C <sub>2</sub> O <sub>3</sub>	→	2CH <sub>3</sub> O <sub>2</sub>				G1
R44b	C <sub>2</sub> O <sub>3</sub> + C <sub>2</sub> O <sub>3</sub> (D)	→	CH <sub>3</sub> O <sub>2</sub> + CH <sub>2</sub> DO <sub>2</sub>			1.000	<sup>b</sup>
R45a	C <sub>2</sub> O <sub>3</sub> + HO <sub>2</sub>	→	CH <sub>3</sub> O <sub>2</sub> + 0.79OH + 0.21ROOH				G1
R45b	C <sub>2</sub> O <sub>3</sub> (D) + HO <sub>2</sub>	→	CH <sub>2</sub> DO <sub>2</sub> <sup>c</sup>			1.000	<sup>b</sup>
R46	PAR + OH	→	0.87XO <sub>2</sub> + 0.76ROR + 0.13XO <sub>2</sub> N + 0.11HO <sub>2</sub> + 0.11ALD2 + 0.11RXPAR				G1
R47	ROR	→	1.10ALD2 + 0.96XO <sub>2</sub> + 0.94HO <sub>2</sub> + 2.10RXPAR				G1
R48	ROR	→	HO <sub>2</sub>				G1
R49a	OLE + OH	→	CH <sub>2</sub> O + ALD2 + XO <sub>2</sub> + HO <sub>2</sub> + RXPAR				G1
R49b	OLE(D) + OH	→	0.500CHDO <sup>c</sup>			1.000	<sup>b</sup>
R50a	OLE + O <sub>3</sub>	→	0.44ALD2 + 0.64CH <sub>2</sub> O + 0.37CO + 0.25HO <sub>2</sub> + 0.29XO <sub>2</sub> + 0.40OH + 0.90RXPAR			4.33 × 10 <sup>-15</sup>	-1800
R50b	OLE(D) + O <sub>3</sub>	→	0.320CHDO <sup>c</sup>			1.000	<sup>b</sup>
R51a	OLE + NO <sub>3</sub>	→	0.91XO <sub>2</sub> + CH <sub>2</sub> O + ALD2 + 0.09XO <sub>2</sub> N + NO <sub>2</sub> + RXPAR			7.7 × 10 <sup>-15</sup>	
R51b	OLE(D) + NO <sub>3</sub>	→	0.320CHDO <sup>c</sup>			1.000	<sup>b</sup>
R52a	ETH + OH	$\xrightarrow{M}$	XO <sub>2</sub> + HO <sub>2</sub> + 1.56CH <sub>2</sub> O + 0.22ALD2				JPL
			<i>k</i> <sub>0</sub>			0.8	
			<i>k</i> <sub>∞</sub>			0.0	
R52b	ETH(D) + OH	→	0.780CHDO <sup>c</sup>			1.000	<sup>b</sup>
R53a	ETH + O <sub>3</sub>	→	CH <sub>2</sub> O + 0.43CO + 0.26HO <sub>2</sub> + 0.12OH			9.1 × 10 <sup>-15</sup>	-2580
R53b	ETH(D) + O <sub>3</sub>	→	0.500CHDO <sup>c</sup>			1.000	<sup>b</sup>
R54	MGLY + OH	→	XO <sub>2</sub> + C <sub>2</sub> O <sub>3</sub>			1.7 × 10 <sup>-11</sup>	
R55	MGLY	$\xrightarrow{h\nu}$	C <sub>2</sub> O <sub>3</sub> + HO <sub>2</sub> + CO				G1
R56a	ISOP + OH	→	0.85XO <sub>2</sub> + 0.61CH <sub>2</sub> O + 0.85HO <sub>2</sub> + 0.03MGLY + 0.58OLE + 0.15XO <sub>2</sub> N + 0.63PAR			2.54 × 10 <sup>-11</sup>	410
R56b	ISOP(D) + OH	→	0.305CHDO <sup>c</sup>			1.000	<sup>b</sup>
R57a	ISOP + O <sub>3</sub>	→	0.90CH <sub>2</sub> O + 0.55OLE + 0.18XO <sub>2</sub> + 0.36CO + 0.15C <sub>2</sub> O <sub>3</sub> + 0.03MGLY + 0.63PAR + 0.30HO <sub>2</sub> + 0.28OH			1.23 × 10 <sup>-14</sup>	-2013
R57b	ISOP(D) + O <sub>3</sub>	→	0.450CHDO <sup>c</sup>			1.000	<sup>b</sup>
R58a	ISOP + NO <sub>3</sub>	→	0.90HO <sub>2</sub> + 0.90ORGNIT + 0.03CH <sub>2</sub> O + 0.45OLE + 0.12ALD + 0.10NO <sub>2</sub> + 0.08MGLY			7.8 × 10 <sup>-13</sup>	
R58b	ISOP(D) + NO <sub>3</sub>	→	0.015CHDO <sup>c</sup>			1.000	<sup>b</sup>

In this table, the rate constants are in molec<sup>*p*</sup> cm<sup>-*q*</sup> s<sup>-1</sup>, with *p* and *q* reaction molecularity dependent. Photolysis rates are wavelength and intensity dependent (see references). CO<sub>2</sub>, O<sub>2</sub> and H<sub>2</sub>O are not listed in reaction products. G1, Gery et al. (1989); G2, Gery et al. (1988); JPL, DeMore et al. (1994); LS, Leone and Seinfeld (1985); SEN, Senum et al. (1984); AT1, Atkinson (1994); WL, Wille et al. (1991); RF, Roberts and Fayer (1989); HT, Hertel et al. (1993); STO, Stockwell et al. (1997); ATG, based on Atkinson (1994) and Gery et al. (1989).

<sup>a</sup> Here the production of HNO<sub>3</sub> is neglected because the small amount of ALD2(D) involved. Actually, C<sub>2</sub>O<sub>3</sub>(D) is not produced and transported as a species but is defined as a fraction of the ALD2 corresponding to an isotopic composition of -86 ‰, i.e. equal to the isotopic composition of CH<sub>4</sub>.

<sup>b</sup> Discussed in Sect. 2.2.

<sup>c</sup> Here the production of other species than CHDO is neglected because the small amount of ALD2(D), C<sub>2</sub>O<sub>3</sub>(D) OLE(D), ETH(D), or ISOP(D) involved. Actually, the deuterated companion species are not produced or transported but are defined as fractions of the non-deuterated species corresponding to an isotopic composition of -86 ‰, i.e. equal to the isotopic composition of CH<sub>4</sub>.

Feilberg et al. (2007a) and Rhee et al. (2008). In absence of established experimental values we adapted a KIE of 1.580 for the radical channel. The KIE for the removal reaction of formaldehyde by OH oxidation (R34) was adopted from Feilberg et al. (2004) and set to 1.280. No kinetic isotope effects are implemented for the reaction of formaldehyde with NO<sub>3</sub> (R35) because of its minor importance in the global H<sub>2</sub> budget.

## Appendix B

### Derivation of the NMHC reaction mechanism

The reaction mechanism for the NMHC's used for this work is shown in Table B1. In this table, ALD2 represents acetaldehyde and higher aldehydes, C<sub>2</sub>O<sub>3</sub> is the peroxyacetyl radical, PAN represents the peroxyacetyl nitrate and

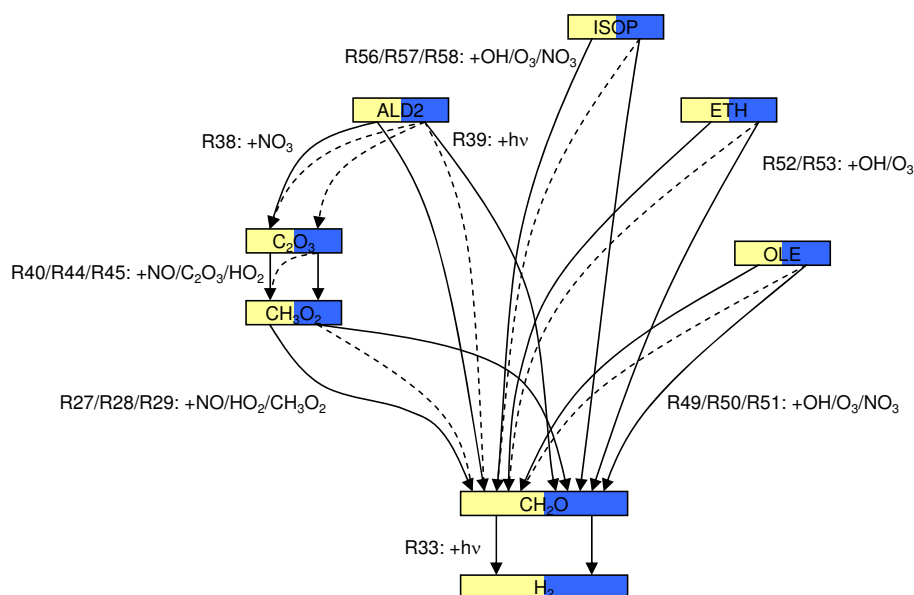


**Fig. B1.** NMHC reactions modified for hydrogen isotope chemistry. Yellow container species are non-deuterated, whereas blue containers species are singly deuterated species. The solid lines indicate production of the species from the reactant species that is taken into account, whereas the dashed lines indicate production that is neglected (as explained in Sect. 2.2).

higher PANs, PAR are the paraffinic carbon atoms, OLE are the olefinic carbon bonds, ETH are the alkenes, MGLY is methylglyoxal, ISOP is isoprene, ROOH represents the lumped organic peroxides ( $> C_1$ ), ORGNIT represents the lumped alkyl nitrates,  $XO_2$  is the NO to  $NO_2$  operator,  $XO_2N$  is the NO to alkyl nitrate operator, and finally RXPAN is the PAR budget corrector. Because experimental data on the full NMHC oxidation chain are not available, and because the isotope effects in the oxidation of singly deuterated NMHCs such as isoprene are expected to be small (e.g., Atkinson et al., 2006; McCaulley et al., 1989), we chose not to incorporate kinetic isotope effects in the standard model parameters at this time (i.e.  $KIE = 1.000$  for all reactions) and subsequently, branching is treated purely statistical.

The branching ratios of the removal reactions of the olefins (OLE), alkenes (ETH), and isoprene (ISOP) by OH,  $O_3$ , and  $NO_3$  (Reactions R49 to R53, R56 to R58) were adopted from Pieterse et al. (2009). Because of the comparable initial amount of hydrogen atoms, the branching ratios of the oxidation and photolysis reactions of acetaldehyde and higher aldehydes (R38 and R39) are assumed to be equal to the branching ratios of ETH and OLE (0.500). The reactions of the important intermediate peroxyacetyl radical ( $C_2O_3$ ) with NO,  $C_2O_3$  and  $HO_2$ , leading to formaldehyde and  $XO_2$  in the original CBM-4 scheme (Reactions R40, R44, and R45, respectively) were altered to produce  $CH_3OO$  instead. This way, the isotope and branching effects in the remaining reactions towards  $H_2$  are taken into account appropriately. The involved reactions are shown schematically in Fig. B1.

## Appendix C

### Derivation of expressions to analyse the variability in the $H_2$ budget

The variability in the  $H_2$  budget can be analysed by taking the time derivative of the definition expression for the  $H_2$  mixing ratio:

$$\frac{d[H_2]}{dt} = \frac{M_{\text{air}}}{M_{H_2}} \left( \frac{1}{m_{\text{air}}} \frac{dm_{H_2}}{dt} - \frac{m_{H_2}}{m_{\text{air}}^2} \frac{dm_{\text{air}}}{dt} \right), \quad (C1)$$

where  $M_{\text{air}}$  and  $M_{H_2}$  are the molar mass of air and  $H_2$ . Furthermore,  $m_{\text{air}}$  and  $m_{H_2}$  are the overall air and  $H_2$  masses in the budget domains. Note that the monthly change in the overall air mass should be considered when studying the variability in the mixing ratio. We have combined this effect into the default horizontal transport budget term in the  $H_2$  budget because it is related to the seasonal cycles in surface pressure (as a result of the seasonal cycle in temperature) above the oceans and continents in the NH and SH that also cause horizontal transport. In general, the change in  $H_2$  (by mass) can be calculated using  $n$  flux terms in the budget for the sources and sinks, resulting in the following expression:

$$\frac{d[H_2]}{dt} = \frac{M_{\text{air}}}{M_{H_2}} \left( \frac{1}{m_{\text{air}}} \sum_{i=0}^{n-1} \frac{dm_{H_2,i}}{dt} - \frac{m_{H_2}}{m_{\text{air}}^2} \frac{dm_{\text{air}}}{dt} \right). \quad (C2)$$

Similarly, we can investigate the variability in the isotope budget of  $H_2$  by using the definition for the isotope ratio:

$$R \equiv \frac{[\text{HD}]}{2[\text{H}_2]}, \quad (\text{C3})$$

to obtain its time derivative in the following form:

$$\frac{dR}{dt} = \frac{1}{2[\text{H}_2]} \frac{d\text{HD}}{dt} - \frac{[\text{HD}]}{2[\text{H}_2]^2} \frac{d\text{H}_2}{dt}. \quad (\text{C4})$$

In general, the time derivatives of the  $\text{H}_2$  and HD mixing ratios are equal to the sum of  $n$  flux terms that can be positive or negative for each of the two isotopologues, also dependent on time. Hence, Eq. (C4) reduces to:

$$\frac{dR}{dt} = \frac{1}{2} \sum_{i=0}^{n-1} \left( \frac{1}{[\text{H}_2]} P_{\text{HD},i} - \frac{[\text{HD}]}{[\text{H}_2]^2} P_{\text{H}_2,i} + \frac{[\text{HD}]}{[\text{H}_2]} (k_{\text{H}_2,i} - k_{\text{HD},i}) \right) \quad (\text{C5})$$

In this expression,  $P_{\text{H}_2,i}$  and  $P_{\text{HD},i}$  are the production flux terms of  $\text{H}_2$  and HD, respectively. The variables  $k_{\text{H}_2,i}$  and  $k_{\text{HD},i}$  are the removal rate coefficients. The impact of source, sink, and bi-directional processes on the variability in the isotope ratio can now be calculated in terms of equally scaled contributions. Moreover, the extension to the delta-notation (isotopic composition) is straightforward:

$$\frac{d}{dt} \delta\text{D}[\text{H}_2] = \frac{d}{dt} \left( \frac{R}{R_{\text{VSMOW}}} - 1 \right) = \frac{1}{R_{\text{VSMOW}}} \frac{dR}{dt}. \quad (\text{C6})$$

#### Supplementary material related to this article is available online at:

<http://www.atmos-chem-phys.net/11/7001/2011/acp-11-7001-2011-supplement.pdf>.

**Acknowledgements.** This study was funded by the Dutch NWO-ACTS project 053.61.026 and by the Eurohydros project, via the Sixth Framework Programme of the European Union (SUSTDEV-2005-3.I.2.1 Atmospheric composition change: Methane, Nitrous Oxide and Hydrogen). Andrew Rice from Portland State University (USA) and Paul Quay from the University of Washington (USA) are acknowledged for providing their  $\text{H}_2$  isotope data. Paul Novelli from NOAA/CMDL (USA) provided the  $\text{H}_2$  measurement data used for the validation of the modelled  $\text{H}_2$  mixing ratios. We would like to thank Laurens Ganzeveld from Wageningen University (NL) for help with the implementation of the dry deposition parametrisation. Finally, the National Computing Facilities foundation (NCF) is acknowledged for providing the computational facilities to run the TM5 model.

Edited by: P. Jöckel

#### References

Appenzeller, C., Davies, H. C., and Norton, W. A.: Fragmentation of stratospheric intrusions, *J. Geophys. Res.*, 101(D1), 1435–1456, doi:10.1029/95JD02674, 1996.  
 Atkinson, R.: Gas-phase tropospheric chemistry of organic compounds, *J. Phys. Chem. Ref. Data Monogr.*, 2, 1–216, 1994.

Atkinson, R., Baulch, D. L., Cox, R. A., Hampson, R. F., Kerr, J. A., and Troe, J.: Evaluated kinetic and photochemical data for atmospheric chemistry: supplement IV, *Atmos. Environ.*, 26, 1187–1230, 1992.  
 Atkinson, R., Baulch, D. L., Cox, R. A., Crowley, J. N., Hampson, R. F., Hynes, R. G., Jenkin, M. E., Rossi, M. J., Troe, J., and IUPAC Subcommittee: Evaluated kinetic and photochemical data for atmospheric chemistry: Volume II – gas phase reactions of organic species, *Atmos. Chem. Phys.*, 6, 3625–4055, doi:10.5194/acp-6-3625-2006, 2006.  
 Batenburg, A. M., Walter, S., Pieterse, G., Levin, I., Schmidt, M., Jordan, A., Hammer, S., Yver, C., and Röckmann, T.: Temporal and spatial variability of the stable isotopic composition of atmospheric molecular hydrogen: observations at six EUROHYDROS stations, *Atmos. Chem. Phys.*, 11, 6985–6999, doi:10.5194/acp-11-6985-2011, 2011.  
 Brühl, C. and Crutzen, P. J.: MPIC two dimensional model, *NASA Ref. Publ.*, 1292, 103–104, 1992.  
 Conrad, R. and Seiler, W.: Contribution of hydrogen production by biological nitrogen fixation to the global hydrogen budget, *J. Geophys. Res.*, 85(C10), 5493–5498, 1980.  
 Conrad, R. and Seiler, W.: Influence of temperature, moisture, and organic carbon on the flux of  $\text{H}_2$  and CO between soil and atmosphere: field studies in subtropical regions, *J. Geophys. Res.*, 90, 5699–5709, 1985.  
 DeMore, W. B., Sander, S. P., Golde, D. M., Hampson, R. F., Kurylo, M. J., Howard, C. J., Ravishankara, A. R., Kolb, C. E., and Molina, M. J.: Chemical kinetics and photochemical data for use in stratospheric modelling, evaluation number 11, Technical report, JPL Publication 94-26, Jet Propulsion Laboratory, Pasadena, 1994.  
 Dethof, A., O'Neill, A., and Slingo, J.: Quantification of the isentropic mass transport across the dynamical tropopause, *J. Geophys. Res.*, 105(D10), 12279–12293, doi:10.1029/2000JD900127, 2000.  
 Ehhalt, D. H.: Gas phase chemistry of the troposphere, in: *Topics Phys. Chem.*, Vol. 6, edited by: Zellner, R., Springer-Verlag, New York, 21–109, 1999.  
 Ehhalt, D. H. and Rohrer, F.: The tropospheric cycle of  $\text{H}_2$ : a critical review, *Tellus B*, 61(3), 500, doi:10.1111/j.1600-0889.2009.00416.x, 2009.  
 Feck, T., Groöß, J.-U., and Riese, M.: Sensitivity of Arctic ozone loss to stratospheric  $\text{H}_2\text{O}$ , *Geophys. Res. Lett.*, 35, L01803, doi:10.1029/2007GL031334, 2008.  
 Feilberg, K. L., Johnson, M. S., and Nielsen, C. J.: Relative reaction rates of HCHO, HCDO, DCDO,  $\text{H}^{13}\text{CHO}$ , and  $\text{HCH}^{18}\text{O}$  with OH, Cl, Br, and  $\text{NO}_3$  radicals, *J. Phys. Chem. A*, 108, 7393–7398, 2004.  
 Feilberg, K. L., D'Anna, B., Johnson, M. S., and Nielsen, C. J.: Relative tropospheric photolysis rates of HCHO,  $\text{H}^{13}\text{CHO}$ ,  $\text{HCH}^{18}\text{O}$ , and DCDO measured at the european photoreactor facility (EUPHORE), *J. Phys. Chem. A*, 109, 8314–8319, 2005.  
 Feilberg, K. L., Johnson, M. S., Bacak, A., Röckmann, T., and Nielsen, C. J.: Relative tropospheric photolysis rates of HCHO and HCDO measured at the European photoreactor facility, *J. Phys. Chem. A*, 111, 9034–9036, 2007a.  
 Feilberg, K. L., D'Anna, B., Johnson, M. S., and Nielsen, C. J.: Additions and Corrections: Relative tropospheric photolysis rates

- of HCHO, H<sup>13</sup>CHO, HCH<sup>18</sup>O, and DCDO measured at the european photoreactor facility (EUPHORE), *J. Phys. Chem. A*, 111(5), p. 992, 2007b.
- Ganzeveld, L. and Lelieveld, J.: Dry deposition parameterization in a chemistry general circulation model and its influence on the distribution of reactive trace gases, *J. Geophys. Res.*, 100(D10), 20999–21012, 1995.
- Ganzeveld, L., Lelieveld, J., and Roelofs, G.-J.: A dry deposition parameterization for sulfur oxides in a chemistry and general circulation model, *J. Geophys. Res.*, 105(D5), 5679–5694, doi:10.1029/97JD03077, 1998.
- Garland, J. A.: The dry deposition of sulphur dioxide to land and water surfaces, *P. R. Soc. London*, A354, 245–268, 1977.
- Gerst, S. and Quay, P.: The deuterium content of atmospheric molecular hydrogen: method and initial measurements, *J. Geophys. Res.*, 105, 26433–26445, 2000.
- Gerst, S. and Quay, P.: Deuterium component of the global molecular hydrogen cycle, *J. Geophys. Res.*, 106, 5021–5031, 2001.
- Gery, M. W., Whitten, G. Z., Killus, J. P., and Dodge, M. C.: Development and testing of the CBM-4 for urban and regional modelling, Technical Report Rep. EPA-600/3-88-012, US Environ. Prot. Agency, Research Triangle Park, NC, 1988.
- Gery, M. W., Whitten, G. Z., Killus, J. P., and Dodge, M. C.: A photochemical kinetics mechanism for urban and regional scale computer modeling, *J. Geophys. Res.*, 94(12), 12925–12956, 1989.
- Hauglustaine, D. A. and Ehhalt, D. H.: A three-dimensional model of molecular hydrogen in the troposphere, *J. Geophys. Res.*, 107, 4330, doi:10.1029/2001JD001156, 2002.
- Hertel, O., Berkowicz, R., Christensen, J., and Hov, O.: Test of two numerical schemes for use in atmospheric transport-chemistry models, *Atmos. Environ.*, 27A, 2591–2611, 1993.
- Hicks, B. B., Hosker, R. P., Myers, T. P., and Womack, J. D.: Dry deposition measurement techniques, I, Design and tests of a prototype meteorological and chemical system for determining dry deposition, *Atmos. Environ.*, 25, 2345–2359, 1991.
- Hintsa, E. J., Boering, K. A., Weinstock, E. M., Anderson, J. G., Gary, B. L., Pfister, L., Daube, B. C., Wofsy, S. C., Loewenstein, M., Podolske, J. R., Margitan, J. J., and Bui, T. P.: Troposphere-to-stratosphere transport in the lowermost stratosphere from measurements of H<sub>2</sub>O, CO<sub>2</sub>, N<sub>2</sub>O and O<sub>3</sub>, *Geophys. Res. Lett.*, 25(14), 2655–2658, doi:10.1029/98GL01797, 1998.
- Houghton, J. T., Ding, Y., Griggs, D. J., Noguier, M., van der Linden, P. J., Dai, X., Maskell, K., and Johnson, C. A.: Chapt. 4: Atmospheric chemistry and greenhouse gases, in: *Climate Change 2001: The Scientific Basis*, Contribution of Working Group I to the Third Assessment Report of the Intergovernmental Panel on Climate Change, edited by: Houghton, J. T., Ding, Y., Griggs, D. J., Noguier, M., van der Linden, P. J., Dai, X., Maskell, K., and Johnson, C. A., Cambridge University Press, Cambridge, UK and New York, NY, USA, 2001.
- Houweling, S., Dentener, F., and Lelieveld, J.: The impact of non-methane hydrocarbon compounds on tropospheric photochemistry, *J. Geophys. Res.*, 103(D9), 10673–10696, 1998.
- Jacobson, M. Z., Colella, W. G., and Golden, D. M.: *Cleaning the Air and Improving Health with Hydrogen Fuel-Cell Vehicles*, Science, 308(5730), 1901–1905, doi:10.1126/science.1109157, 2005.
- Krol, M., Houweling, S., Bregman, B., van den Broek, M., Segers, A., van Velthoven, P., Peters, W., Dentener, F., and Bergamaschi, P.: The two-way nested global chemistry-transport zoom model TM5: algorithm and applications, *Atmos. Chem. Phys.*, 5, 417–432, doi:10.5194/acp-5-417-2005, 2005.
- Lawrence, M. G., Jöckel, P., and von Kuhlmann, R.: What does the global mean OH concentration tell us?, *Atmos. Chem. Phys.*, 1, 37–49, doi:10.5194/acp-1-37-2001, 2001.
- Lelieveld, J., Bregman, B., Arnold, F., Bürger, V., Crutzen, P. J., Fischer, H., Waibel, A., Siegmund, P., and van Velthoven, P. F. J.: Chemical perturbation of the lowermost stratosphere through exchange with the troposphere, *Geophys. Res. Lett.*, 24(5), 603–606, doi:10.1029/97GL00255, 1997.
- Leone, J. A. and Seinfeld, J. H.: Comparative analysis of chemical reaction mechanisms for photochemical smog, *Atmos. Environ.*, 19, 437–464, 1985.
- Mar, K. A., McCarthy, M. C., Connell, P., and Boering, K. A.: Modeling the photochemical origins of the extreme deuterium enrichment in stratospheric H<sub>2</sub>, *J. Geophys. Res.*, 112, D19302, doi:10.1029/2006JD007403, 2007.
- McCarthy, M. C., Boering, K. A., Rahn, T., Eiler, J., Rice, A., Tyler, S. C., and Atlas, E.: The hydrogen isotopic composition of water vapor entering the stratosphere inferred from high precision measurements of δD-CH<sub>4</sub> and δD-H<sub>2</sub>, *J. Geophys. Res.*, 109, D07304, doi:10.1029/2003JD004003, 2004.
- McCaulley, J. A., Kelly, N., Golde, M. F., and Kaufman, F.: Kinetic studies of the reactions of F and OH with CH<sub>3</sub>OH, *J. Phys. Chem.*, 93, 1014–1018, 1989.
- Meirink, J. F., Bergamaschi, P., Frankenberg, C., d'Amelio, M. T. S., Dlugokencky, E. J., Gatti, L. V., Houweling, S., Miller, J. B., Röckmann, T., Villani, M. G., and Krol, M. C.: Four-dimensional variational data assimilation for inverse modelling of atmospheric methane emissions: Analysis of SCIAMACHY observations, *J. Geophys. Res.*, 113, D17301, doi:10.1029/2007JD009740, 2008a.
- Meirink, J. F., Bergamaschi, P., and Krol, M. C.: Four-dimensional variational data assimilation for inverse modelling of atmospheric methane emissions: method and comparison with synthesis inversion, *Atmos. Chem. Phys.*, 8, 6341–6353, doi:10.5194/acp-8-6341-2008, 2008b.
- Meyers, T. P., Finkelstein, P., Clarke, J., Ellestad, T. G., and Sims, P. F.: A multilayer model for inferring dry deposition using standard meteorological measurements, *J. Geophys. Res.*, 103(D17), 22645–22661, 1998.
- Moortgat, G. K., Klippel, W., Mobius, K. H., Seiler, W., and Warneck, P.: MPIC two dimensional model, Technical Report Rep. FAA-EE-80-47, US Dept. of Transp., Washington, DC, USA, 1980.
- Nilsson, E. J. K., Johnson, M. S., Taketani, F., Matsumi, Y., Hurley, M. D., and Wallington, T. J.: Atmospheric deuterium fractionation: HCHO and HCDO yields in the CH<sub>2</sub>DO + O<sub>2</sub> reaction, *Atmos. Chem. Phys.*, 7, 5873–5881, doi:10.5194/acp-7-5873-2007, 2007.
- Nilsson, E. J. K., Andersen, V. F., Skov, H., and Johnson, M. S.: Pressure dependence of the deuterium isotope effect in the photolysis of formaldehyde by ultraviolet light, *Atmos. Chem. Phys.*, 10, 3455–3462, doi:10.5194/acp-10-3455-2010, 2010.
- Novelli, P. C., Lang, P. M., Masarie, K. A., Hurst, D. F., Myers, R., and Elkins, J. W.: Molecular hydrogen in the troposphere: Global distribution and budget, *J. Geophys. Res.*, 104, 30427–

- 30444, 1999.
- Olivier, J. G. J. and Berdowski, J. J. M.: Global emissions sources and sinks, in: *The Climate System*, edited by: Berdowski, J., Guicherit, R., and Heij, B. J., A.A. Balkema Publishers/Swets & Zeitlinger Publishers, Lisse, The Netherlands, 2001.
- Pieterse, G., Krol, M. C., and Röckmann, T.: A consistent molecular hydrogen isotope chemistry scheme based on an independent bond approximation, *Atmos. Chem. Phys.*, 9, 8503–8529, doi:10.5194/acp-9-8503-2009, 2009.
- Pieterse, G., Krol, M. C., Popa, E., Vermeulen, A. T., van den Bulk, P., Jongejan, P., Batenburg, A. M., and Röckmann, T.: Comparing two-way nested TM5 model results for molecular hydrogen with background and continental measurements, in preparation, 2011.
- Price, H., Jaeglé, L., Rice, A., Quay, P., Novelli, P. C., and Gammon, R.: Global budget of molecular hydrogen and its deuterium content: constraints from ground station, cruise, and aircraft observations, *J. Geophys. Res.*, 112, D22108, doi:10.1029/2006JD008152, 2007.
- Quay, P., Stutsman, J., Wilbur, D., Snover, A., Dlugokencky, E., and Brown, T.: The isotopic composition of atmospheric methane, *Global Biogeochem. Cy.*, 13, 445–461, 1999.
- Rahn, T., Eiler, J. M., Kitchen, N., Fessenden, J. E., and Rander-son, J. T.: Concentration and  $\delta D$  of molecular hydrogen in boreal forests: ecosystem-scale systematics of atmospheric  $H_2$ , *Geophys. Res. Lett.*, 29, 1888, doi:10.1029/2002GL015118, 2002a.
- Rahn, T., Kitchen, N., and Eiler, J. M.: D/H ratios of atmospheric  $H_2$  in urban air: results using new methods for analysis of nano-molar  $H_2$  samples, *Geochim. Cosmochim. Ac.*, 66, 2475–2481, 2002b.
- Rahn, T., Eiler, J. M., Boering, K. A., Wennberg, P. O., McCarthy, M. C., Tyler, S., Schauffler, S., Donnelly, S., and Atlas, E.: Extreme deuterium enrichment in stratospheric hydrogen and the global atmospheric budget of  $H_2$ , *Nature*, 424, 918–921, 2003.
- Rahn, T., Randerson, J. T., and Eiler, J.: Variability of Deuterium Fractionation Associated With Soil Uptake of Atmospheric Molecular Hydrogen, *Eos Trans. AGU*, 86(52), Fall Meet. Suppl., Abstract B11A-1031, 2005.
- Ravishankara, A. R.: Kinetics of radical reactions in the atmospheric oxidation of  $CH_4$ , *Annu. Rev. Phys. Chem.*, 39, 367–394, 1988.
- Rayleigh, L.: On the distillation of binary mixtures, *Philos. Mag.*, 4(23), 521–537, 1902.
- Reid, S. J. and Vaughan, G.: Lamination in ozone profiles in the lower stratosphere, *Q. J. Roy. Meteorol. Soc.*, 117, 825–844, 1991.
- Rhee, T. S., Brenninkmeijer, C. A. M., and Röckmann, T.: The overwhelming role of soils in the global atmospheric hydrogen cycle, *Atmos. Chem. Phys.*, 6, 1611–1625, doi:10.5194/acp-6-1611-2006, 2006.
- Rhee, T. S., Brenninkmeijer, C. A. M., and Röckmann, T.: Hydrogen isotope fractionation in the photolysis of formaldehyde, *Atmos. Chem. Phys.*, 8, 1353–1366, doi:10.5194/acp-8-1353-2008, 2008.
- Rice, A., Quay, P., Stutsman, J., Gammon, R., Price, H., and Jaeglé, L.: Meridional distribution of molecular hydrogen and its deuterium content in the atmosphere, *J. Geophys. Res.*, 115, D12306, doi:10.1029/2009JD012529, 2010.
- Roberts, J. M. and Fayer, R. W.: UV absorption cross section of organic nitrates of potential atmospheric importance and estimation of atmospheric lifetimes, *Environ. Sci. Technol.*, 23, 945–951, 1989.
- Röckmann, T., Rhee, T. S., and Engel, A.: Heavy hydrogen in the stratosphere, *Atmos. Chem. Phys.*, 3, 2015–2023, doi:10.5194/acp-3-2015-2003, 2003.
- Röckmann, T., Walter, S., Bohn, B., Wegener, R., Spahn, H., Brauers, T., Tillmann, R., Schlosser, E., Koppmann, R., and Rohrer, F.: Isotope effect in the formation of  $H_2$  from  $H_2CO$  studied at the atmospheric simulation chamber SAPHIR, *Atmos. Chem. Phys.*, 10, 5343–5357, doi:10.5194/acp-10-5343-2010, 2010a.
- Röckmann, T., Gómez Álvarez, C. X., Walter, S., Veen, C. v., Wollny, A. G., Gunthe, S. S., Helas, G., Pöschl, U., Keppler, F., Greule, M., and Brand, W. A.: The isotopic composition of  $H_2$  from wood burning - dependency on combustion efficiency, moisture content and  $\delta D$  of local precipitation, *J. Geophys. Res.*, 115, D17308, doi:10.1029/2009JD013188, 2010b.
- Sander, S. P., Finlayson-Pitts, B. J., Friedl, R. R., Golden, D. M., Huie, R. E., Keller-Rudek, H., Kolb, C. E., Kurylo, M. J., Molina, M. J., Moortgat, G. K., Orkin, V. L., R., R. A., and Wine, P. H.: *Chemical Kinetics and Photochemical Data for Use in Atmospheric Studies*, Evaluation Number 15, Technical Report, JPL Publication 06-2, Jet Propulsion Laboratory, Pasadena, 2006.
- Sanderson, M. G., Collins, W. J., Derwent, R. G., and Johnson, C. E.: Simulation of global hydrogen levels using a lagrangian three dimensional model, *J. Atmos. Chem.*, 46, 15–28, 2003.
- Schmidt, H. L., Werner, R. A., and Eisenreich, W. (2003): Systematics of  $^2H$  patterns in natural compounds and its importance for the elucidation of biosynthetic pathways, *Phytochem. Rev.*, 2, 61–85, 2003.
- Schultz, M. and Stein, O.: GEMS (GRG) emissions for 2003 reanalysis simulations, Technical report, MPI-M, Max Planck Institute for Meteorology, Hamburg, Germany, 2006.
- Schultz, M. G., Diehl, T., Brasseur, G. P., and Zittel, W.: Air pollution and climate-forcing impacts of a global hydrogen economy, *Science*, 302, 624–627, 2003.
- Seiler, W. and Conrad, R.: Contribution of tropical ecosystems to the global budgets for trace gases, especially  $CH_4$ ,  $H_2$ , CO and  $N_2O$ , in: *The Geophysiology of Amazonia: Vegetation and Climate Interactions*, edited by: Dickerson, R., John Wiley, New York, 33–62, 1987.
- Senum, G. I., Lee, Y. N., and Gaffney, J. S.: Ultraviolet absorption spectrum of peroxy acetyl nitrate and peroxy propionyl nitrate, *J. Phys. Chem.*, 88, 1269–1270, 1984.
- Stockwell, W. R., Kirchner, F., Kuhn, M., and Seefeld, S.: A new mechanism for regional atmospheric chemistry modeling, *J. Geophys. Res.*, 102, 25847–25879, 1997.
- Tromp, T. K., Shia, R.-L., Allen, M., Eiler, J. M., and Yung, Y. L.: Potential environmental impact of a hydrogen economy on the stratosphere, *Science*, 300, 1740–1742, 2003.
- van den Broek, M. M. P., van Aalst, M. K., Bregman, A., Krol, M., Lelieveld, J., Toon, G. C., Garcelon, S., Hansford, G. M., Jones, R. L., and Gardiner, T. D.: The impact of model grid zooming on tracer transport in the 1999/2000 Arctic polar vortex, *Atmos. Chem. Phys.*, 3, 1833–1847, doi:10.5194/acp-3-1833-2003, 2003.

- van Noije, T. P. C., Eskes, H. J., van Weele, M., and van Velthoven, P. F. J.: Implications of the enhanced Brewer-Dobson circulation in European Centre for Medium-Range Weather Forecasts reanalysis ERA-40 for the stratosphere-troposphere exchange of ozone in global chemistry transport models, *J. Geophys. Res.*, 109, D19308, doi:10.1029/2004JD004586, 2004.
- van Noije, T. P. C., Segers, A. J., and van Velthoven, P. F. J.: Time series of the stratosphere-troposphere exchange of ozone simulated with reanalyzed and operational forecast data, *J. Geophys. Res.*, 111, D03301, doi:10.1029/2005JD006081, 2006.
- Vollmer, M. K., Walter, S., Bond, S. W., Soltic, P., and Röckmann, T.: Molecular hydrogen ( $H_2$ ) emissions and their isotopic signatures (H/D) from a motor vehicle: implications on atmospheric  $H_2$ , *Atmos. Chem. Phys.*, 10, 5707–5718, doi:10.5194/acp-10-5707-2010, 2010.
- Walter, S., Laukenmann, S., Siemerink, M. A. J., Vollmer, M. K., Gleixner, G., and Röckmann, T.: The stable isotopic signature of biologically produced molecular hydrogen, in preparation, 2011.
- Warneck, P.: *Chemistry of the natural atmosphere*, Int. Geophys. Ser., Academic, San Diego, Calif., 757 pp., 1988.
- Warwick, N. J., Bekki, S., Nisbet, E. G., and Pyle, J. A.: Impact of a hydrogen economy on the stratosphere and troposphere studied in a 2-D model, *Geophys. Res. Lett.*, 31, L05107, doi:10.1029/2003GL019224, 2004.
- Wille, U., Becker, E., Schindler, R. N., Lancer, I. T., Poulet, G., and LeBras, G.: A discharge flow mass-spectrometric study of the reaction of the  $NO_3$  radical and isoprene, *J. Atmos. Chem.*, 13, 183–193, 1991.
- Xiao, X., Prinn, R. G., Simmonds, P. G., Steele, L. P., Novelli, P. C., Huang, J., Langenfelds, R. L., O'Doherty, S., Krummel, P. B., Fraser, P. J., Porter, L. W., Weiss, R. F., Salameh, P., and Wang, R. H. J.: Optimal estimation of the soil uptake of molecular hydrogen from the advanced global atmospheric gases experiments and other measurements, *J. Geophys. Res.*, 112, D07303, doi:10.1029/2006JD007241, 2007.
- Yonemura, S., Kawashima, S., and Tsuruta, H.: Carbon monoxide, hydrogen, and methane uptake by soils in a temperate arable field and a forest, *J. Geophys. Res.*, 105(D11), 14347–14362, 2000.
- Yashiro, H., Sudo, K., Yonemura, S., and Takigawa, M.: The impact of soil uptake on the global distribution of molecular hydrogen: chemical transport model simulation, *Atmos. Chem. Phys. Discuss.*, 11, 4059–4103, doi:10.5194/acpd-11-4059-2011, 2011.